

**CERTS MICROGRID: MODELING,
ANALYSIS AND CONTROL OF
DISTRIBUTED ENERGY RESOURCES — PHASE I**

Ajit A. Renjit, Mahesh S. Illindala, Abrez Mondal

Department of Electrical and Computer Engineering

The Ohio State University

Columbus, OH 43210

Technical Report Prepared under Subcontract No. 7004227

Lawrence Berkeley National Laboratory

December 2015

Acknowledgments

The work described in this report was coordinated by the Consortium for Electric Reliability Technology Solutions, and funded by the Office of Electricity Delivery and Energy Reliability, Power Systems Engineering R&D Program of the U.S. Department of Energy through a Subcontract #7004227 with The Ohio State University administered by the Lawrence Berkeley National Laboratory.

Specifically, the authors would like to thank Robert H. Lasseter, University of Wisconsin-Madison, Joseph H. Eto, Lawrence Berkeley National Laboratory, and Benjamin L. Schenkman, Sandia National Laboratory for unfailing support and encouragement. This work would not have been possible without the sharing of knowledge, experience and field-testing carried out at the CERTS Microgrid test bed in AEP Dolan Technology Center, Groveport, OH by David A. Klapp and Amrit S. Khalsa.

Executive Summary

Introduction:

A microgrid provides the framework for integration and coordination of distributed energy resources (DERs). The aim of this work is to develop dynamic models for two kinds of prime-mover driven DERs — synchronous generator-based DER (also known as ‘genset’) and inverter-based DER — installed at the CERTS Microgrid in AEP Dolan Technology Center, Groveport, OH. Such models could be used in analyzing various system scenarios including large-scale distribution systems, which maybe otherwise impractical to do actual testing due to resource limitations in the field test bed.

Problem Identification:

The microgrid can work either in the grid-connected or islanded mode. However, the islanded mode of operation presents many challenges to the microgrid survivability. In particular, adverse conditions are observed in an islanded microgrid when large and fluctuating loads are supplied from several smaller-rated DERs. Similar consequences follow the loss of generation in the microgrid causing a large change in net load to the surviving DERs. If any of these DERs cannot sustain the net load change, they lead the microgrid system to a cascading failure.

Conclusion:

In this work, it was discovered that a large electrical load demand, sometimes even within the DER kW-rating, can result in its prime-mover stalling. This is because every engine is rated for maximum torque, or in other words, the mechanical power production

capability of engine is derated at lower speeds. Due to the lower inertia of DERs employed in a microgrid system, their prime-mover speed undergoes huge swings upon a large disturbances. The root cause of stalling behavior is the slow response of the engine governor that restores the prime-mover speed following a load change.

In a synchronous generator-based DER (i.e., genset), the prime-mover speed is proportional to the DER's frequency. Hence, the stalling in genset causes a frequency collapse in the microgrid. By contrast, the prime-mover stalling in an inverter-based DER results in a voltage collapse. This is because the inverter-based DER has an additional power conditioning stage after the permanent magnet synchronous generator (PMSG).

When multiple DERs are integrated in a microgrid, these DERs are expected to share with each other their surplus marginal capacity so that no one will get overloaded. However, this did not happen in a particular test carried out at the CERTS Microgrid, i.e., a mixed source microgrid comprising genset and inverter-based DER. It was found that the slow acting governor controls of genset did not rescue the inverter-based DER from its prime-mover stalling. A large load change caused voltage collapse in the inverter-based DER and led to a cascading failure of the microgrid.

Recommendation:

To avoid the DER prime-mover stalling in a microgrid, the CERTS P_{\max} controls can be applied. Otherwise, a modified active power-frequency ($P-\omega$) droop controller is a viable option for an inverter-based DER that is sharing load together with a genset. Besides, prime-mover stalling could be prevented by making design changes to engine governor controls. The ultimate goal is to improve DER coordination in the microgrid.

Thesis and Publications

- [P1] A. A. Renjit, "Modeling, Analysis and Control of Mixed Source Microgrid," Ph.D. Dissertation, Electrical and Computer Engineering, The Ohio State University, Columbus, OH, Dec. 2015.
- [P2] A. A. Renjit, M. S. Illindala, and D. A. Klapp, "Graphical and Analytical Methods for Stalling Analysis of Engine Generator Sets," *IEEE Trans. Ind. Appl.*, vol. 50, no. 5, pp. 2967–2975, Sep. 2014.
- [P3] A. A. Renjit and M. S. Illindala, "Graphical and analytical methods for stalling of engine generator set," in *Power Electronics, Drives and Energy Systems (PEDES), 2012 IEEE International Conference on*, Dec. 2012, pp. 1–6.
- [P4] A. A. Renjit, M. S. Illindala, R. H. Lasseter, M. J. Erickson, and D. Klapp, "Modeling and control of a natural gas generator set in the CERTS microgrid," in *Energy Conversion Congress and Exposition (ECCE), 2013 IEEE*, 2013, pp. 1640–1646.
- [P5] A. Mondal, M. S. Illindala, A. A. Renjit, and A. S. Khalsa, "Analysis of limiting bounds for stalling of natural gas genset in the CERTS microgrid test bed," in *Power Electronics, Drives and Energy Systems (PEDES), 2014 IEEE International Conference on*, Dec. 2014, pp. 1–5.
- [P6] A. A. Renjit, M. S. Illindala, and D. A. Klapp, "Modeling and analysis of the CERTS microgrid with natural gas powered distributed energy resources," in *Industrial & Commercial Power Systems Technical Conference (I&CPS), 2015 IEEE/IAS 51st*, 2015, pp. 1–8.

Table of Contents

Executive Summary	ii
Table of Contents	v
List of Tables	viii
List of Figures	ix
CHAPTER 1 MODELING OF RECIPROCATING ENGINE DRIVEN DISTRIBUTED ENERGY RESOURCES	1
1.1 Introduction.....	1
1.2 CERTS Microgrid Test Bed – System Description	1
1.3 Modeling of Synchronous Generator-based Distributed Energy Resource (i.e., Genset).....	3
1.4 Modeling of Inverter-based Distributed Energy Resource	10
1.5 Summary	14
CHAPTER 2 ANALYSIS OF PRIME-MOVER STALLING IN RECIPROCATING ENGINE DRIVEN DISTRIBUTED ENERGY RESOURCES	16
2.1 Introduction.....	16
2.2 Prime-mover Stalling in a Synchronous Generator-based Distributed Energy Resource	16

2.3 Stalling Analysis of Synchronous Generator-based DERs with Load Relief Scheme.....	23
2.4 Prime-mover Stalling in an Inverter-based Distributed Energy Resource..	26
2.5 Effect of Incremental Load Change on Prime-mover Stalling	34
2.6 Comparison Between Synchronous Generator-based DERs and Inverter-based DERs.....	36
2.7 Summary	36
CHAPTER 3 DER OPERATION AT LIMITING CONDITIONS IN AN ISLANDED MICROGRID.....	38
3.1 Introduction.....	38
3.2 Load Sharing Between Two Gensets in a Microgrid at Limiting Conditions	38
3.3 Load Sharing in a Mixed Source Microgrid Under Limiting Conditions...	45
3.4 Why is the Underfrequency Load Relief (V/Hz) Scheme not used in Gensets for Operation in Microgrid?	52
3.5 Summary	54
CHAPTER 4 CONTROL AND PREVENTION OF PRIME-MOVER STALLING IN DISTRIBUTED ENERGY RESOURCES	55
4.1 Introduction.....	55
4.2 Analysis of DER Prime-mover Stalling in a Mixed Source Microgrid.....	56

4.3 Prevention of DER Prime-mover Stalling in a Mixed Source Microgrid...	61
4.4 Prevention of DER Prime-mover Stalling Through Governor Controls	67
4.5 Summary	69
CHAPTER 5 CONCLUSION AND FUTURE WORK	70
5.1 Conclusion	70
5.2 Suggested Future Work.....	72
Appendix A.....	74
Appendix B	76
References.....	78

List of Tables

Table 2.1 Calculated values of $NL - lim1$ & $\omega L - lim1$ for different step load changes.....	22
Table 2.2 Synchronous generator-based DERs vs. inverter-based DERs	36
Table 4.1 Difference between the frequency response of traditional and modified P - ω droop controller.....	62
Table 4.2 Lead/lag transfer function based modified droop controller settings	63

List of Figures

Figure 1.1 Simplified schematic illustrating the interconnection of natural gas engine driven DERs at the CERTS Microgrid test bed	2
Figure 1.2 Controller architecture of MTU Onsite Energy natural gas engine driven synchronous generator-based DER (or ‘genset’).....	4
Figure 1.3 Genset performance with isochronous governor for a 0 – 80 kW step change in electrical load. Experimental waveforms are presented on the left column and the corresponding simulation results are on the right column.	9
Figure 1.4 Control architecture of the inverter-based DER model. (a) Natural gas engine driven PMSG prime-mover, and (b) integration of CERTS controls into power conditioning system (PCS).	11
Figure 1.5 Inverter-based DER performance for a 0-94 kW step change in electrical load. Experimental waveforms are shown on the left column and the corresponding simulation results are on the right column.....	14
Figure 2.1 Block diagram of the electromechanical energy conversion process in a synchronous generator-based DER (i.e., genset).....	17
Figure 2.2 Fuel map of GM 8.1L natural gas engine [31]	18
Figure 2.3 Speed vs. active power characteristics of the genset for a 0–70 kW step load application.....	20

Figure 2.4 Locus of the active power-speed characteristics of the genset for 90% (i.e. 0–90 kW) step load application.	23
Figure 2.5 Experimental plots showing the genset response with load relief (V/Hz) scheme for a 20–95 kW step change in electrical load.....	25
Figure 2.6 Locus of the speed vs. active power characteristics of the genset with load relief (V/Hz) scheme for 20–95 kW step load application.....	26
Figure 2.7 An inverter-based distributed energy resource (DER). (a) Simplified schematic, and (b) block diagram of the electromechanical energy conversion process.	27
Figure 2.8 Locus of the PMSG speed and voltage vs. active power for the inverter-based DER in response to a 0–94 kW step load application.....	29
Figure 2.9 Inverter-based DER output characteristics for a 0–94 kW step load application. (a) PCS output voltage (V_{ac2} , RMS value) vs. active power, and (b) PCS output frequency vs. active power.	31
Figure 2.10 Locus of the PMSG speed and voltage vs. active power for the inverter-based DER in response to a 0–70 kW step load application.....	32
Figure 2.11 Inverter-based DER output characteristics for a 0–70 kW step load application. (a) PCS output voltage (V_{ac2} , RMS value) vs. active power, and (b) PCS output frequency vs. active power.	33
Figure 2.12 Locus of speed vs. active power for (a) genset with 70–90 kW load change, and (b) inverter-based DER with 60–94 kW load change.	35

Figure 3.1 Schematic illustrating the interconnection of two gensets in an islanded microgrid.....	39
Figure 3.2 Genset-1 (a) Steady state speed governor droop characteristics with $P_{ref1} = 0$ kW, and (b) locus of the active power-speed response for a 20–90 kW step load application.....	40
Figure 3.3 Genset-2 (a) Steady state speed governor droop characteristics with $P_{ref2} = 40$ kW, and (b) locus of the active power-speed response for a 20–90 kW step load application.....	41
Figure 3.4 Schematic illustrating the interconnection of two gensets in the islanded microgrid. The transient load sharing between gensets is affected by droop gains as well as transient reactances (Xd').	43
Figure 3.5 Load sharing among Genset-1 and Genset-2. (a) Steady state speed governor droop characteristics, and (b) locus of the active power-speed response for a 40–180 kW step load application.....	44
Figure 3.6 Schematic of the mixed source microgrid comprising synchronous generator-based and inverter-based DERs.....	46
Figure 3.7 Simulation results illustrating the system performance for a load change from 75 kW to 150 kW. DER-1 (genset in blue): isochronous governor; DER-2 (inverter-based DER in red): $P_{ref2} = 0$ kW, $P_{max2} = 100$ kW.	47
Figure 3.8 Experimental results illustrating the system performance for a load change from 75 kW to 150 kW. DER-1 (genset in blue): isochronous governor; DER-2 (inverter-based DER in red): $P_{ref2} = 0$ kW, $P_{max2} = 100$ kW.	48

Figure 3.9 Steady state load sharing between DER-1 and DER-2 for a load change from 75 kW to 150 kW. DER-1 (genset): isochronous governor; DER-2 (inverter-based DER): $P_{ref2} = 0$ kW, $P_{max2} = 100$ kW..... 49

Figure 3.10 Simulation results illustrating the system performance for a load change from 75 kW to 150 kW. DER-1 (genset in blue): $P_{ref1} = 75$ kW, $P_{max1} = 93$ kW; DER-2 (inverter-based DER in red): $P_{ref2} = 0$ kW, $P_{max2} = 100$ kW. 50

Figure 3.11 Experimental results illustrating the system performance for a load change from 75 kW to 150 kW. DER-1 (genset in blue): $P_{ref1} = 75$ kW, $P_{max1} = 93$ kW; DER-2 (inverter-based DER in red): $P_{ref2} = 0$ kW, $P_{max2} = 100$ kW..... 51

Figure 3.12 Steady state load sharing between DER-1 and DER-2 for a load change from 75 kW to 150 kW. DER-1 (genset): isochronous governor; DER-2 (inverter-based DER): $P_{ref2} = 0$ kW, $P_{max2} = 100$ kW..... 52

Figure 3.13 Experimental results illustrating the system performance for a load change from 75 kW to 150 kW. DER-1 (genset in blue): $P_{ref1} = 0$ kW, $P_{max1} = 100$ kW, and load relief (V/Hz) is enabled; DER-2 (inverter-based DER in red): $P_{ref2} = 0.75$ kW, $P_{max2} = 100$ kW..... 54

Figure 4.1 Schematic of the mixed source microgrid comprising inverter- and synchronous generator-based DERs. 56

Figure 4.2 Experimental results showing the performance of the DERs for a load change from 75 kW to 150 kW. DER-1 (genset in red): isochronous governor; DER-2 (inverter-based DER in blue): $P_{ref2} = 37.5$ kW, $P_{max2} = 100$ kW. 58

Figure 4.3 Simulation results showing the performance of the DERs for a load change from 75 kW to 150 kW. DER-1 (genset in red): isochronous governor; DER-2 (inverter-based DER in blue): $P_{ref2} = 37.5$ kW, $P_{max2} = 100$ kW.	59
Figure 4.4 Simulation plot showing the frequency collapse in the genset (DER-1) of the mixed source microgrid for a 75–150 kW step load application.	60
Figure 4.5 Locus of the PMSG speed and voltage vs. power characteristics for the inverter-based DER (DER-2) in the mixed source microgrid for a 75–150 kW step load application.....	60
Figure 4.6 Block diagram of inverter-based DER’s modified power-frequency (P- ω) droop controller using lead/lag controls	62
Figure 4.7 Transient and steady state frequency droop curves of the inverter-based DER with modified power-frequency (P- ω) controls.....	63
Figure 4.8 Simulation plots illustrating the system dynamic response for a 75–150 kW step change in electrical load. DER-1 (genset in red): isochronous governor; DER-2 (inverter-based DER in blue): $P_{ref2} = 37.5$ kW, $P_{max2} = 100$ kW.	64
Figure 4.9 Locus of the PMSG speed and voltage vs. power characteristics for the inverter-based DER in the mixed source microgrid for a 75–150 kW step load application	65
Figure 4.10 Results showing the performance of the proposed controller for 75–150 kW load change. DER ₁ (synchronous generator in red): isochronous governor; DER ₂ (inverter in blue): $P_{ref2} = 37.5$ kW, $P_{max2} = 100$ kW. See Figure 4.8 for the description of event ⑦.	66

Figure 4.11 Locus of the genset speed vs. power characteristics for a 0–90 kW step load application. Governor PID controller’s proportional gain is set at (a) $K_{pg1} = 15$, and (b) $K_{pg1} = 24$ 68

CHAPTER 1

MODELING OF RECIPROCATING ENGINE DRIVEN DISTRIBUTED ENERGY RESOURCES

1.1 Introduction

This chapter presents the modeling of two kinds of natural gas powered distributed energy resources (DERs), viz., synchronous generator-based and inverter-based DERs, installed at the CERTS Microgrid test bed.

1.2 CERTS Microgrid Test Bed – System Description

The *Consortium of Electric Reliability Technology Solutions* (CERTS) Microgrid test bed was established at the American Electric Power Dolan Technology Center to test the commercial off-the-shelf DERs for plug-and-play operation, peer-to-peer coordination, and seamless islanding and reconnection capabilities [1]–[3]. An overview of the CERTS Microgrid test bed, consisting of three natural gas powered combined heat and power (CHP) DERs manufactured by Tecogen®, is given in [1]. All the three units were at first inverter-based DERs with the CERTS controls [4]–[6]. Later, one of these units was replaced with a synchronous generator-based DER (also known as ‘genset’) manufactured by MTU Onsite Energy®. This is because gensets are popular and affordable to many customers. A simplified schematic of the CERTS Microgrid test bed is illustrated in Figure 1.1, where the system under study is shaded in green color.

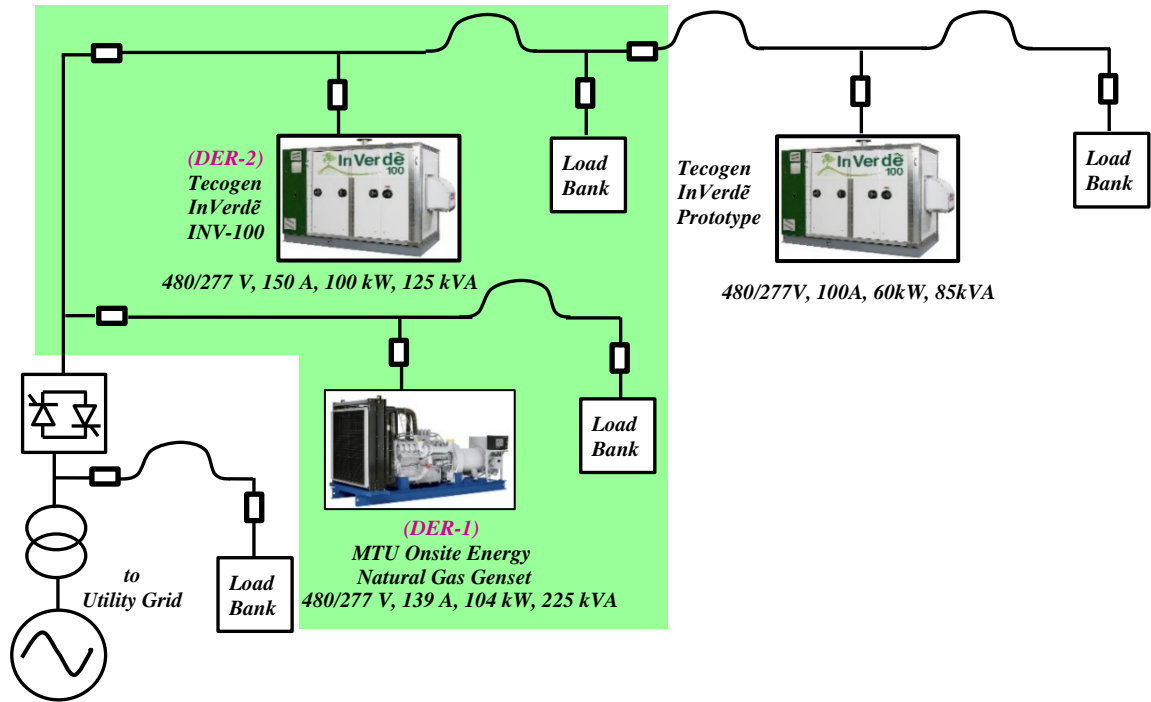


Figure 1.1 Simplified schematic illustrating the interconnection of natural gas engine driven DERs at the CERTS Microgrid test bed

It should be noted that the models for all the components installed at the CERTS Microgrid test bed were developed in MATLAB®/Simulink™/SimPowerSystems toolbox using a black-box approach with only publicly disclosed information and empirical knowledge supported by observed facts from the several tests carried out. The aim is to find simple system models that show the dynamic behavior without infringing on the confidential information of the commercial equipment manufacturers. Such models can be easily multiplied wherever necessary with proper scaling to help analyze various scenarios that maybe otherwise impractical, expensive and time consuming for undertaking a full scale field-testing.

1.3 Modeling of Synchronous Generator-based Distributed Energy Resource (i.e., Genset)

The model of an engine generator set (or genset) has many subsystems that represent its physical behavior. Typically, the genset has a reciprocating engine coupled to the synchronous generator through a mechanical shaft [7]. The engine speed is regulated using an isochronous governor, and the synchronous generator's field circuit is controlled by a brushless exciter. Figure 1.2 displays the detailed control architecture of the MTU Onsite Energy® genset. In the CERTS Microgrid test bed, the MTU Onsite Energy® natural gas powered genset (i.e., DER-1) has a GM 8.1L, 496cc engine (with 8.1L displacement and 4-cycle) with an electronic isochronous speed governor. The output voltage of generator is regulated through a Basler DECS-250 digital voltage regulator (DVR), which can be programmed with adjustable load relief (V/Hz) characteristics. The genset model parameters are given in Appendix A.

1.3.1 *Engine speed governor*

A majority of commercial off-the-shelf gensets come with an electronic isochronous governor. This governor can be modeled by a proportional–integral–derivative (PID) controller that regulates the engine speed, ω_1 , to match the generator speed reference set-point, ω_{ref1} . During a load change, it helps adjust the fuel intake of the engine cylinders. Thus, the output of the governor is the desired fuel quantity to be delivered to generate the required torque.

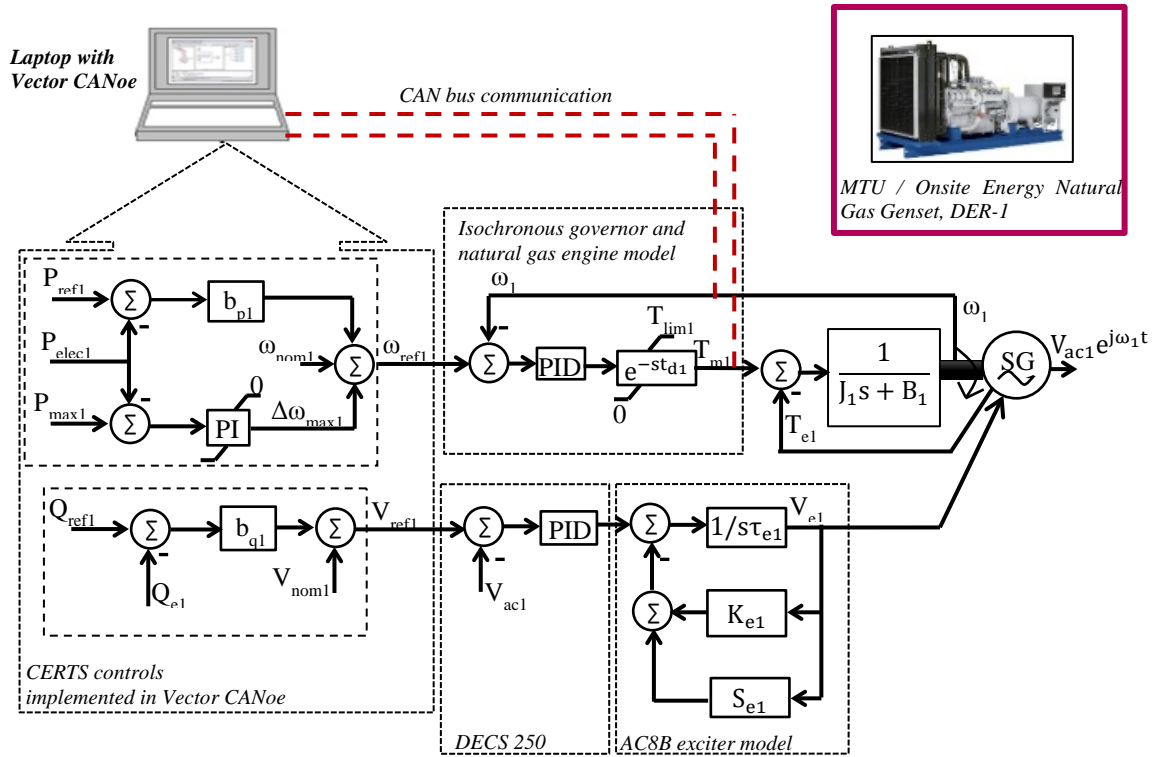


Figure 1.2 Controller architecture of MTU Onsite Energy natural gas engine driven synchronous generator-based DER (or ‘genset’).

1.3.2 Natural gas engine

An alteration in the fuel quantity does not cause a change of engine torque at once. In natural gas engines, an inherent delay exists between the fuel flow (out of the intake manifold of the engine) and the actual torque production. This time delay is comprised of different lags in the fuel delivery and combustion process. The total delay calculation between fuel intake and torque production for a four stroke engine is given by the following equation [8]:

$$t_{d1} = \left(\frac{60}{n_1}\right) \left(1 + \frac{1}{n_{cyl1}}\right) + \left(\frac{45}{6n_1}\right) \quad (1.1)$$

where n_1 denotes the speed of the engine in rpm and n_{cyl1} indicates the number of cylinders in the engine. The delay function $e^{-st_{d1}}$ can be approximated for linear time invariant (LTI) analysis. Generally, a first-order lag function $\frac{1}{1+st_{d1}}$ is a reasonable approximation for LTI analysis. In this case, however, it was found that the first-order Pade approximation $\frac{1-st_{d1}/2}{1+st_{d1}/2}$ gave better results that matched with the manufacturer's test data. Hence, the engine delay is approximated as

$$e^{-st_{d1}} = \frac{1 - st_{d1} / 2}{1 + st_{d1} / 2} \quad (1.2)$$

However, it should be noted that for more precise modeling of the engine, the exponential time delay function (i.e., $e^{-st_{d1}}$) block available in MATLAB®/Simulink™ is recommended in the simulation. Further, the developed mechanical torque, T_{m1} , of the engine is limited to its maximum capacity given by the fuel map. This map is programmed as a torque limiter (saturation) in the model.

1.3.3 *Mechanical coupling shaft*

The next block in Figure 1.2 is the coupling shaft connecting the natural gas engine and the synchronous generator. For the coupling shaft, the rotary motion is expressed by the equation:

$$\omega_1(s)(J_1s + B_1) = T_{m1}(s) - T_{e1}(s) \quad (1.3)$$

where J_1 denotes the net moment of inertia, and B_1 is the net friction loss coefficient of the overall genset assembly.

1.3.4 Digital voltage regulator (DVR) and exciter

The voltage subsystem of the genset comprises the excitation system and digital voltage regulator (DVR). In this subsystem, the generator's field circuit is excited by an AC brushless excitation system that is modeled using AC8B IEEE model [9]. It should be noted that the exciter has a separate alternator with a rotating rectifier to give its dc field supply — called the rotating field exciter. The DVR is modeled as a PID controller for regulating the terminal voltage of the genset. Additional features like the load relief (V/Hz) scheme can also be programmed in the DVR. The model parameters of DVR and exciter are listed in the Appendix A.

Initially, the Marathon Electric's DVR2000E was used to regulate the terminal voltage of the genset. However, it was found to be constraining the load relief to a minimum non-zero value (and not allow programming '0' V/Hz). Hence, it was replaced with Basler's DECS-250 DVR [10] in the experiments conducted later. The purpose of disabling the load relief scheme (by programming '0' V/Hz) is to prevent reactive power circulation between gensets in the microgrid. This problem is discussed further in Section 3.4 of Chapter 3 in this report.

1.3.5 Synchronous generator

The synchronous generator based DER installed at the CERTS microgrid has a salient pole rotor with a rotating field excitation system. It is modeled using the standard block available in the MATLAB®/Simulink™ and SimPowerSystems toolbox library. It has two control inputs, ω_1 and V_{e1} , coming from the governor and exciter, respectively. The generator parameters, given in [11], are programmed in this simulation block.

1.3.6 CERTS controls

The genset model, illustrated in Figure 1.2, also includes an outer loop containing CERTS controls. These controls are used for generating the references to speed governor and exciter. In addition to the power-frequency (P- ω) droop controller, the CERTS controls also have a maximum power (i.e., P_{\max}) controller — to assure that the power supplied by the DER does not exceed its rated maximum capability [2]. However, the P_{\max} controller engages only when the measured active power exceeds the programmed $P_{\max1}$ value (cf. Figure 1.2), and is inactive during the remaining period. An advantage of the flexibility in programming the $P_{\max1}$ parameter is the ability to constrain the DER's steady state output power below its engine rating. Likewise, the reactive power-voltage (Q-V) droop controller is for reactive power sharing when the genset is interconnected with other DERs.

1.3.7 Data acquisition system at the CERTS Microgrid

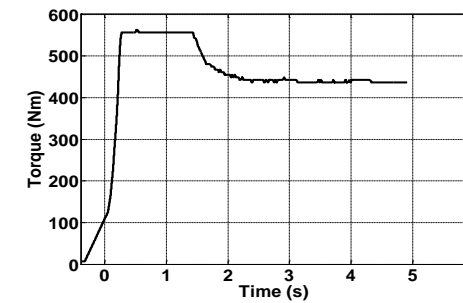
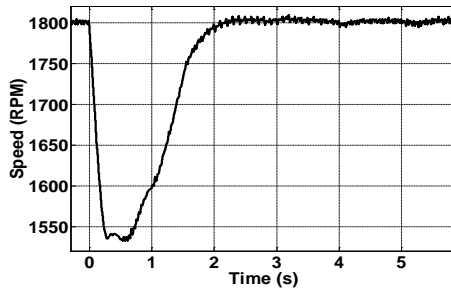
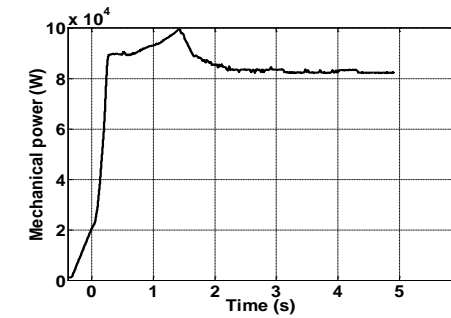
The data acquisition system at the CERTS Microgrid makes use of LabVIEW® for communication with the genset. Three-phase voltages and currents are measured and recorded with real time stamps by PowerLogic® ION7650 metering equipment at various places in the microgrid. Besides them, the internal variables of engine control unit (ECU) of governor were also monitored through the control area network (CAN) bus using Vector CANoe® software. Furthermore, the hardware-in-loop (HIL) feature of Vector CANoe® was utilized to program the CERTS droop controls described earlier. For this purpose, the MATLAB®/Simulink™ Real-Time Workshop™ was used to compile a MATLAB model into a Windows® DLL file that Vector CANoe® can execute.

1.3.8 *Synchronous generator-based DER model validation*

To validate the genset model (cf. Figure 1.2), standalone tests were carried out at the CERTS Microgrid test bed [12]–[14]. The computer simulation in MATLAB®/Simulink™ was done using the ODE 23tb solver, and the dynamic behavior was evaluated for various operating conditions. Figure 1.3 shows selected results that illustrates a close match between simulation waveforms and experimental test data for a 0 – 80 kW step change in load. It should be noted that the CERTS controls are inactive in this particular case.

Prior to the load change, the engine torque and the load torque are equal (i.e., $T_{m1} - T_{e1} = 0$, neglecting losses) and the genset runs at its nominal speed. Yet, after the 80 kW load is applied to the generator, the net torque becomes negative (i.e., $T_{m1} - T_{e1} < 0$) leading to a drop in generator speed. One thing to note is that the speed did not drop instantly due to the generator inertia. Nonetheless, the speed was restored back to its nominal value over time by the isochronous governor. Minor discrepancies between the simulation and experimental waveforms shown in Figure 1.3 are due to un-modeled generator core losses, stray losses and mechanical losses (including friction and windage losses) that vary as a function of speed.

Experimental Waveforms



Simulation Results

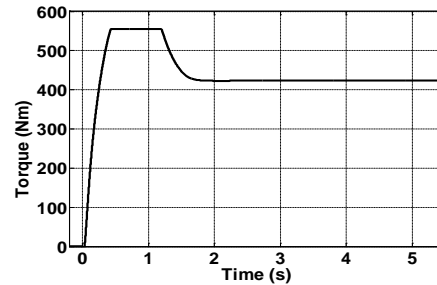
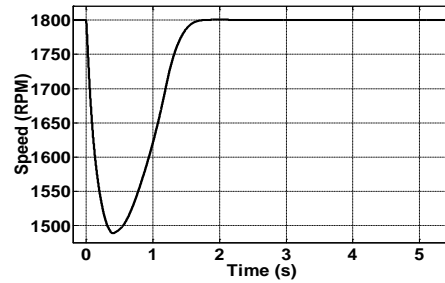
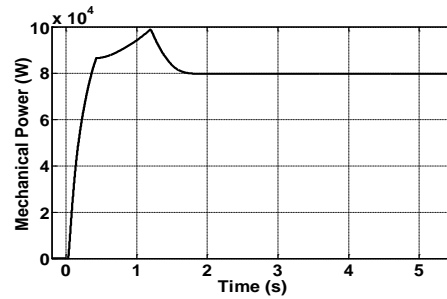


Figure 1.3 Genset performance with isochronous governor for a 0 – 80 kW step change in electrical load. Experimental waveforms are presented on the left column and the corresponding simulation results are on the right column.

1.4 Modeling of Inverter-based Distributed Energy Resource

The synchronous generator-based DER, described in the earlier section, is always run at fixed speed corresponding to the frequency of power delivered to the customers. However, such an operation forces the engine prime-mover to operate outside its optimum fuel efficiency envelope under low load condition [15]–[17]. This results in increased fuel consumption and higher emissions of the engine. Moreover, these gensets often show fluctuations in their frequency and voltage [12], [18]–[21], and even stall sometimes [12], [22], [23] when a large load change occurs.

To overcome the above problems, the inverter-based DERs with a variable speed engine generator set as the prime-mover was proposed [15]–[17], [24]–[26]. In such DERs, the engine speed can be controlled to optimize fuel consumption and reduce emissions [16], [17]. Since the engine is connected to a permanent magnet synchronous generator (PMSG), the variable speed operation of PMSG produces a variable frequency and voltage output. This is converted into a high quality 60 Hz output voltage using power electronics.

At the CERTS Microgrid test bed, the inverter-based DER (labeled as DER-2 in Figure 1.1) is the 100-kW Tecogen® CHP unit, InVerdē INV-100 [4]–[6]. It has a natural gas engine running at variable speed and driving a permanent magnet synchronous generator (PMSG) [4]–[6], [27]. A power conditioning system (PCS) — including diode-bridge rectifier, dc/dc boost converter and dc/ac inverter — converts the variable voltage/frequency output of the generator into a high quality 60 Hz ac power supply [6].

In the natural gas engine, any change in fuel input is reflected in the mechanical torque. However, it does not happen immediately; and it is constrained by factors like fuel transport delay, turbocharger time constant and availability of sufficient combustion air. Therefore, the natural gas engine is modeled as an exponential time delay [8]. In addition, the engine fuel map limits the developed mechanical torque within its maximum rated capacity.

Since the shaft of PMSG is coupled to the natural gas engine, assuming a near linear voltage regulation curve [29], the output voltage is given by the equation

$$V_{pmsg2} = k_e \omega_{pmsg2} \quad (1.4)$$

where ω_{pmsg2} is the prime-mover speed and k_e denotes the emf constant of the generator. A major distinction in using the PMSG in the inverter-based DER is that it does not have a DVR to regulate its terminal voltage as its field circuit excitation is controlled by the permanent magnets in the rotor.

1.4.2 *Power conditioning system (PCS)*

The PMSG gives a variable voltage/frequency ac output that needs a power conditioning system (PCS) to interface with the utility. The PCS includes a diode-bridge rectifier, dc/dc boost converter and dc/ac inverter. Besides, the PCS converts the variable ac output from PMSG into a high quality 60 Hz ac voltage through an LC filter and a coupling inductance [5].

Under normal operating conditions, the PCS inverter's dc bus voltage is regulated by the dc/dc boost converter to decouple the prime-mover voltage (V_{pmsg2}) from the dc/ac

inverter output (V_{ac2}). However, the relationship between these two voltages is non-linear, and so it was found empirically and programmed as a look-up table in the model.

1.4.3 *CERTS controls*

For the inverter-based DER, the CERTS controls are programmed within the PCS as shown in Figure 1.4. They include active power-frequency ($P-\omega$) droop controller, P_{max} controller and reactive power-voltage ($Q-V$) droop controller. It should be noted that the P_{max2} controller remains inactive all the time except when the measured active power exceeds the P_{max2} parameter. An advantage of the flexibility in programming the P_{max2} parameter is the ability to constrain the DER's steady state output below its power rating.

1.4.4 *Inverter-based DER model validation*

To validate the model for inverter-based DER, experimental tests were carried out at the CERTS Microgrid test bed [1]. A particular case of 0–94 kW step load change caused prime-mover stalling event that led to voltage collapse [14]. Figure 1.5 shows the results from both experimental testing and the simulation model for this case.

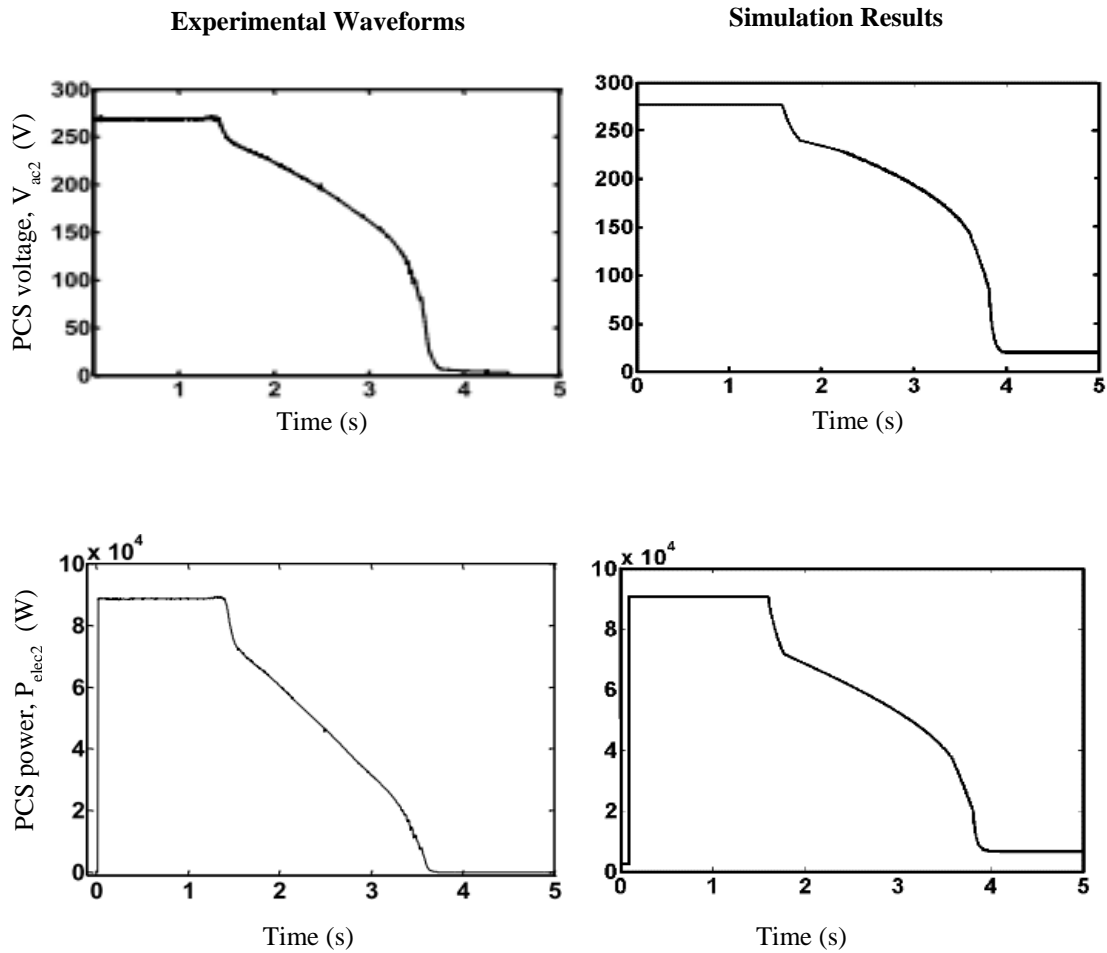


Figure 1.5 Inverter-based DER performance for a 0-94 kW step change in electrical load. Experimental waveforms are shown on the left column and the corresponding simulation results are on the right column.

1.5 Summary

This chapter presented the modeling of the two common types of reciprocating engine driven DERs installed at the CERTS Microgrid test bed, viz., synchronous generator- and inverter-based DERs. The simulation models in MATLAB®/Simulink™ were validated against results from experimental testing. The developed DER models are simple

physics-based models that show to a reasonable degree of accuracy the dynamic behavior without infringing on the confidential information of the equipment manufacturers. Such models can be easily scaled and multiplied to analyze various microgrid scenarios that maybe otherwise impractical to carry out testing on-site due to resource limitations.

CHAPTER 2

ANALYSIS OF PRIME-MOVER STALLING IN RECIPROCATING ENGINE DRIVEN DISTRIBUTED ENERGY RESOURCES

2.1 Introduction

For supplying large and varying loads, the general practice is to oversize the prime-movers of reciprocating engine driven DERs. Otherwise, an abrupt change in the load may cause a significant fluctuation in frequency or voltage. Under extremely harsh load conditions, the DER prime-mover would stall and lead the system to a frequency/voltage collapse. Hence, it is important to investigate the root cause of prime-mover stalling in these DERs. For this purpose, the physics-based models developed in the earlier chapter for the gensets and inverter-based DERs are used.

2.2 Prime-mover Stalling in a Synchronous Generator-based Distributed Energy Resource

Consider the energy conversion process illustrated in Figure 2.1 for a synchronous generator-based DER (i.e., genset). As seen in this figure, the electromechanical energy conversion process in the synchronous generator can be expressed by the following dynamic equation [30]

$$\left(\begin{array}{c} \text{Mechanical Energy Input} \\ \text{from Engine} \end{array} \right) = \left(\begin{array}{c} \text{Electrical Energy} \\ \text{Output} \end{array} \right) + \left(\begin{array}{c} \text{Energy} \\ \text{Dissipated} \end{array} \right) + \left(\begin{array}{c} \text{Increase in Kinetic} \\ \text{Energy, } \Delta KE \end{array} \right)$$

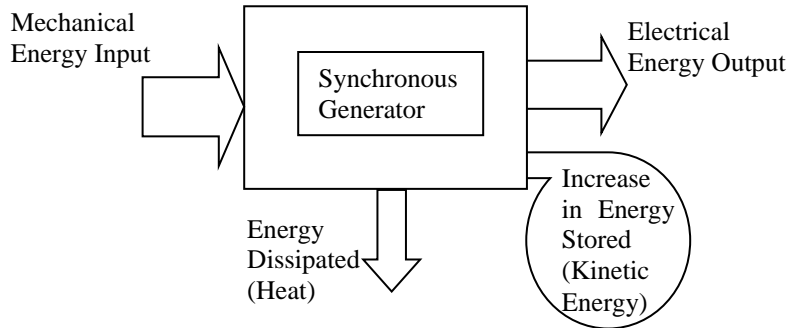
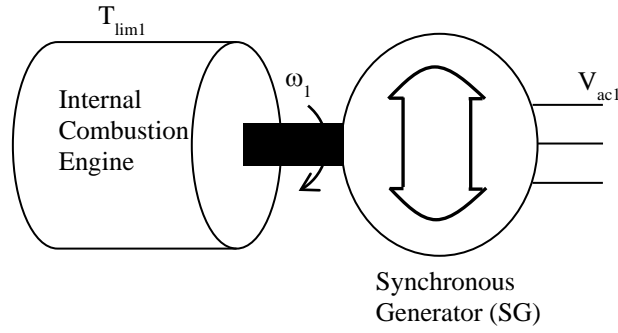


Figure 2.1 Block diagram of the electromechanical energy conversion process in a synchronous generator-based DER (i.e., genset)

In terms of the power quantities, the above dynamic equation can be written as [12]

$$\frac{\Delta KE_1}{\Delta t} = P_{mech1} - P_{elec1} - P_{loss1} \quad (2.1)$$

$$J_1 \omega_1 \frac{\Delta \omega_1}{\Delta t} = P_{mech1} - P_{elec1} - P_{loss1} \quad (2.2)$$

where P_{mech1} is the mechanical input power of generator, P_{elec1} is its electrical output power, and P_{loss1} accounts for the total power losses including copper losses, core losses, stray losses, and friction and windage losses. However, in the first phase of modeling, these losses are neglected. Under steady state conditions, the change in generator speed $\Delta \omega_1$ is zero; as such, the left hand side of the (2.2) will become zero.

At first, the generator is on no-load and rotating at synchronous speed (ω_{syn1}); so its rotational kinetic energy (KE_{init1}) can be computed. Then, from the instant of step change in electrical load (P_{elec1}), equation (2.1) would give the change in kinetic energy (ΔKE_1) over time interval (Δt). Thus, the additional load is temporarily supplied by the stored rotational kinetic energy until the governor action raises the mechanical power (P_{mech1}) to match with P_{elec1} . However, P_{mech1} is limited by the prime-mover's maximum power capability (MP_{max1}) given by the engine fuel map shown in Figure 2.2. Hence, if $P_{elec1} > P_{mech1}$ for a long duration, the stored kinetic energy is drained at the rate given by (2.1). This also causes the generator's speed to drop as per (2.2). For simplicity, it is assumed that MP_{max1} varies linearly with speed. This means that the mechanical torque limit (T_{lim1} , cf. Figure 2.2) is almost constant.

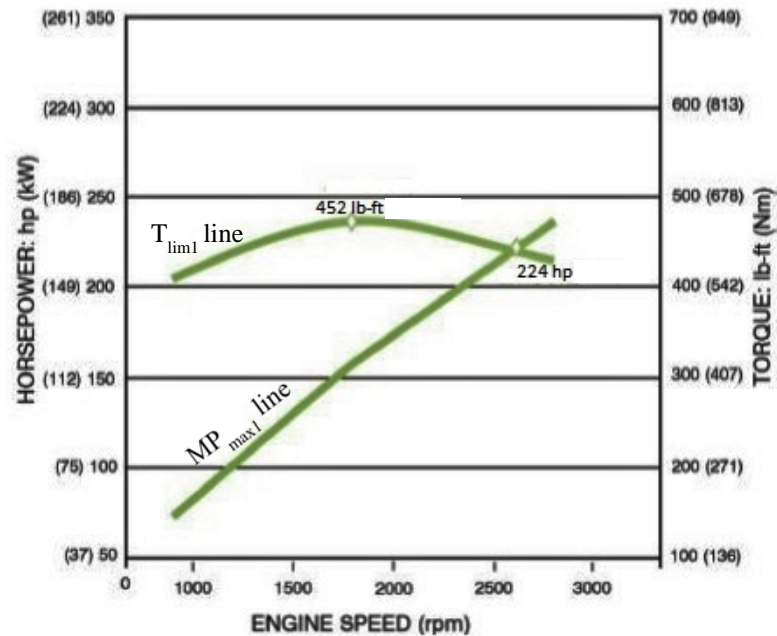


Figure 2.2 Fuel map of GM 8.1L natural gas engine [31]

2.2.1 *Case study*

The case of a step load application to the genset, dealt in earlier chapter (cf. Figure 2.3) is studied further. When a large electrical load (P_{elec1}) is applied to the synchronous generator, its speed (ω_1) reduces briefly until the governor PID controller restores to the desired value. The governor increases the fuel input to the cylinders of the engine, which then generates the necessary mechanical power (P_{mech1}) to compensate for the increase in P_{elec1} . However, the engine fuel map limits the maximum mechanical torque supplied by the engine to T_{lim1} . As seen in Figure 2.3, T_{lim1} from both simulation and experimental results is around 552 Nm. A theoretical approximation for T_{lim1} can be derived by assuming the slope of the power curve of engine fuel map in Figure 2.2, to be a straight line. This approximation is valid over a speed range, and T_{lim1} is computed from its fuel map as

$$T_{lim1} = \frac{104.0 [kW]}{188.5 [rad/s]} = 552.04 Nm \quad (2.3)$$

Figure 2.3 illustrates the locus of speed vs. active power characteristics of the genset for a step change in electrical load of 0–70 kW. The electrical load (P_{elec1}) trajectory is indicated in blue color as P_{elec1} . By contrast, the mechanical power ($P_{mech1} - P_{loss1}$) trajectory follows the green color path. The governor controls gradually restore the speed that dropped because of load change. An additional time (engine delay) is necessary to increase fuel input to the engine cylinders. Hence, the energy balance equation (cf. (2.1)) forces $\Delta KE_1 \neq 0$, thereby causing a speed variation in the transient; this is indicated by the two (blue and green) trajectories going through different paths in Figure 2.3.

However, both the trajectories eventually converge in the equilibrium (i.e., steady state) conditions, when $\Delta KE_1 = 0$; and under these conditions (2.1) becomes

$$P_{mech1.ss} = P_{elec1.ss} + P_{loss1.ss} \text{ (in steady state)} \quad (2.4)$$

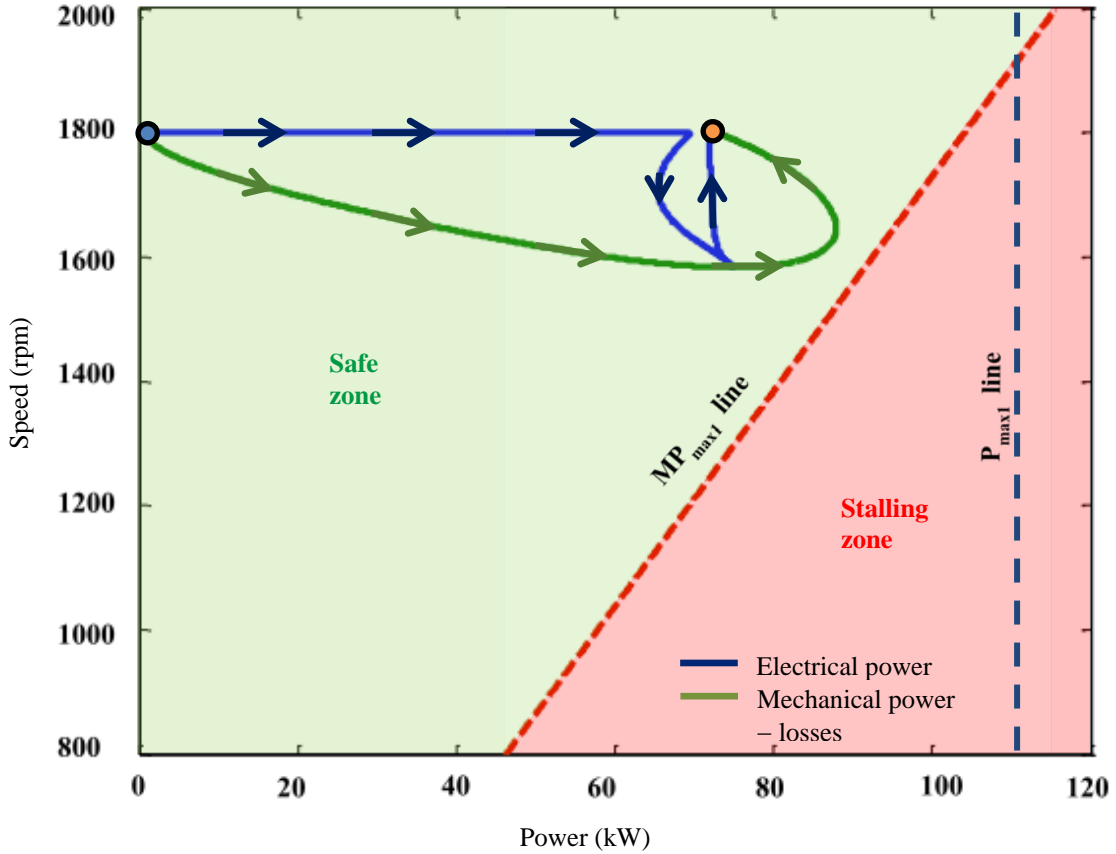


Figure 2.3 Speed vs. active power characteristics of the genset for a 0–70 kW step load application

2.2.2 Conditions for prime-mover stalling

In the locus of genset speed vs. active power shown in Figure 2.3, the mechanical power trajectory would never cross the engine fuel map limit (MP_{max1}) [12]. Hence, the MP_{max1} line also indicates the boundary between *Stalling zone* and *Safe zone*. By contrast, the electrical load shared by the genset with other DERs in the network could be

limited to P_{max1} value by the CERTS P_{max} controller. Nevertheless, if the electrical power trajectory remains in the *Safe zone*, then the genset speed is restored to the equilibrium value without prime-mover stalling.

$$\text{i.e.,} \quad MP_{max1} > P_{elec1} + P_{loss1} \quad (2.5)$$

since P_{mech1} is constrained by the fuel map limit (MP_{max1}). However, as seen in Figure 2.3, MP_{max1} has a linear relationship with speed (ω_1). In other words

$$MP_{max1} = T_{lim1} \omega_1 \quad (2.6)$$

Substituting (2.6) in (2.5), the condition for genset to not stall is

$$\begin{aligned} T_{lim1} \omega_1 &> P_{elec1} + P_{loss1} \\ \text{i.e.,} \quad \omega_1 &> \frac{P_{elec1} + P_{loss1}}{T_{lim1}} \end{aligned} \quad (2.7)$$

The right hand side of (2.7) is denoted by ω_{L-lim1} . Hence,

$$\omega_1 > \omega_{L-lim1} \quad (2.8)$$

Converting the units of ω_{L-lim1} from rad./s to rev./min. (i.e., rpm), the lower limit of speed for the genset to be restored to equilibrium without stalling is given by

$$N_{L-lim1} [rpm] = \frac{P_{elec1}[W] + P_{loss1}[W]}{T_{lim1}[Nm]} \times \frac{60}{2\pi} \quad (2.9)$$

The calculated values of ω_{L-lim1} and N_{L-lim1} are tabulated in Table 2.1 for two large load demands. As seen in Figure 2.3, the *Safe zone* region (shaded in green) satisfies (2.8). The restoration of speed to the equilibrium can be guaranteed by running the genset in the *Safe zone*. Since the genset operation remained in the *Safe zone* when it was subjected to a 0–70 kW step load, its speed was restored to the equilibrium in steady state.

Table 2.1 Calculated values of N_{L-lim1} & ω_{L-lim1} for different step load changes

Applied load, P_{elec1} [kW]	$\omega_{L-lim1} \left[\frac{rad}{sec} \right]$	$N_{L-lim1} [rpm] = \omega_{L-lim} * \frac{60}{2\pi}$
0–70 kW	$\frac{70 \text{ kW}}{552.0371 \text{ Nm}} = 126.8 \frac{rad}{s}$	1210.88 rpm
0–90 kW	$\frac{90 \text{ kW}}{552.0371 \text{ Nm}} = 163.043 \frac{rad}{s}$	1556.951 rpm

However, if the genset leaves the *Safe zone* and enters the *Stalling zone*, it would not attain equilibrium steady state speed. The *Stalling zone* is indicated by the region shaded in red in Figure 2.4, the locus of speed vs. active power for a 0–90 kW step load application. As seen in the figure, the mechanical power trajectory did not cross the MP_{max1} line, as it cannot exceed the engine fuel map limit. When the electrical power trajectory entered the *Stalling zone* (shaded in red), it cannot be met by the engine whose mechanical power production is limited by the fuel map. During this prolonged power mismatch, the genset's stored kinetic energy is depleted, thereby resulting in prime-mover stalling condition [12].

Another way to examine the prime-mover stalling is by defining the new variable of electrical load torque,

$$T_{L-elec1} = \frac{P_{elec1} + P_{loss1}}{\omega_1} \quad (2.10)$$

It follows that the condition for the genset to be restored to equilibrium without stalling, i.e., (2.8) is equivalent to

$$T_{L-elec1} < T_{lim1} \quad (2.11)$$

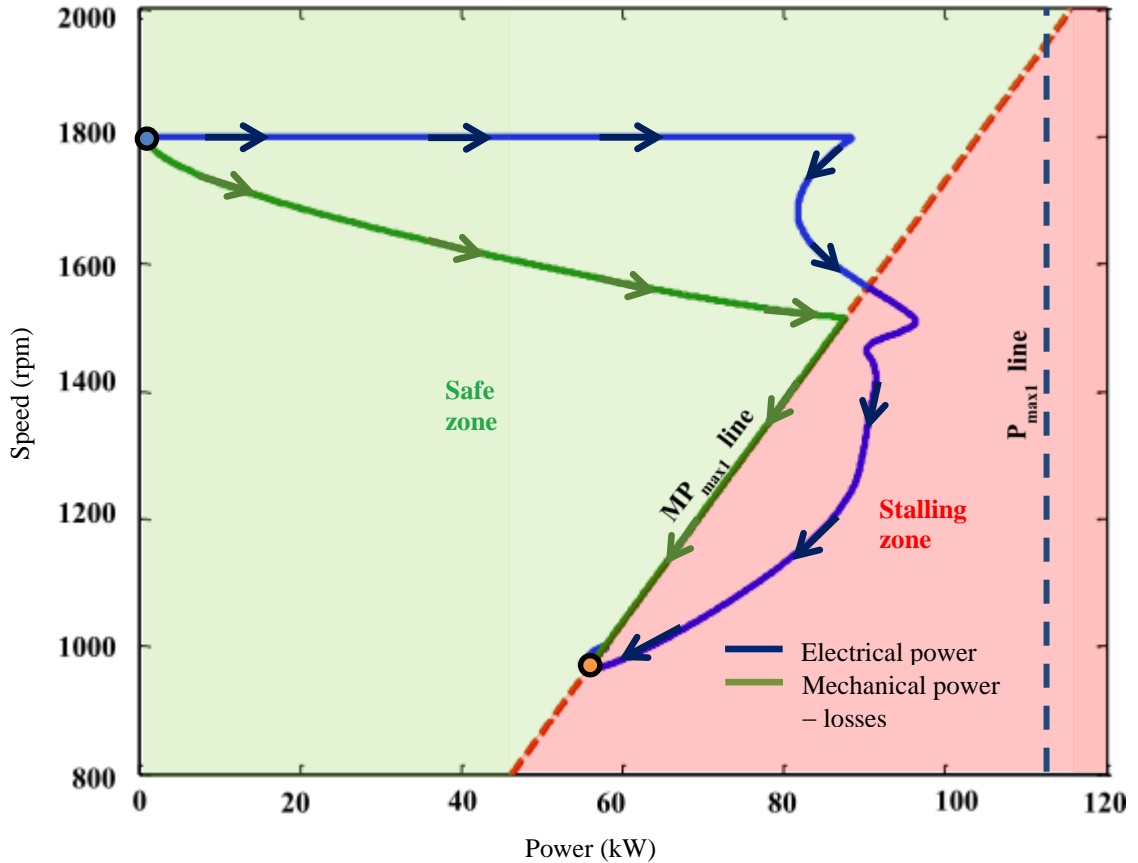


Figure 2.4 Locus of the active power-speed characteristics of the genset for 90% (i.e. 0–90 kW) step load application.

2.3 Stalling Analysis of Synchronous Generator-based DERs with Load Relief Scheme

The analysis of prime-mover stalling in gensets, illustrated in previous section (i.e., Section 2.2), assumed that the genset exciter has no underfrequency load relief (V/Hz) scheme. However, in the standalone mode of operation an underfrequency load relief (V/Hz) scheme could prevent the genset from the stalling condition. In fact, several large

commercial-off-the-shelf gensets meant for standalone operation have DVRs with this programmable option [20].

Figure 2.5 illustrates the genset response for a 20–95 kW step change in electrical load with load relief setting at 3 pu V/Hz [12]. Earlier, it was shown that a 0–90 kW load change, when applied without the load relief (V/Hz) scheme, caused prime-mover stalling in the genset. However, a 3pu V/Hz load relief setting in the DVR reduced the voltage with the speed drop during the time 0–2 s, and this led to an electrical load relief as seen in the measured three-phase power plotted in Figure 2.5. In particular, a decrease in speed from 1800 rpm to 1580 rpm caused a 33% decrease from 277 Vrms to 187 Vrms in the generator terminal voltage. This temporary voltage reduction resulted in a corresponding decrease in the effective electrical load by almost 48% (from 95 kW to 50 kW). The load relief helped in enforcing a gradual increase in load demand rather than an abrupt one, thus giving adequate time for the natural gas engine to respond. In due course, the engine speed was restored to the nominal value of 1800 rpm and the generator terminal voltage and the electrical load returned to their desired values.

Figure 2.6 shows the genset speed vs. active power characteristics of the genset with load relief (V/Hz) scheme for 20–95 kW step load application. Since the genset operation remained in the *Safe zone*, its speed was restored to the equilibrium in steady state.

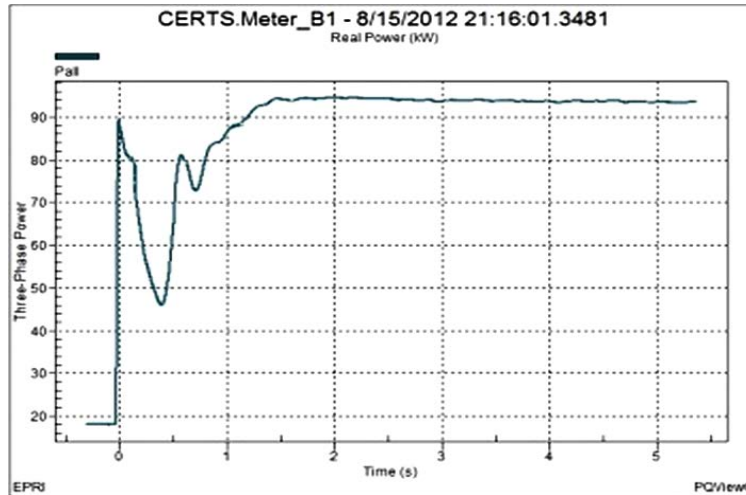
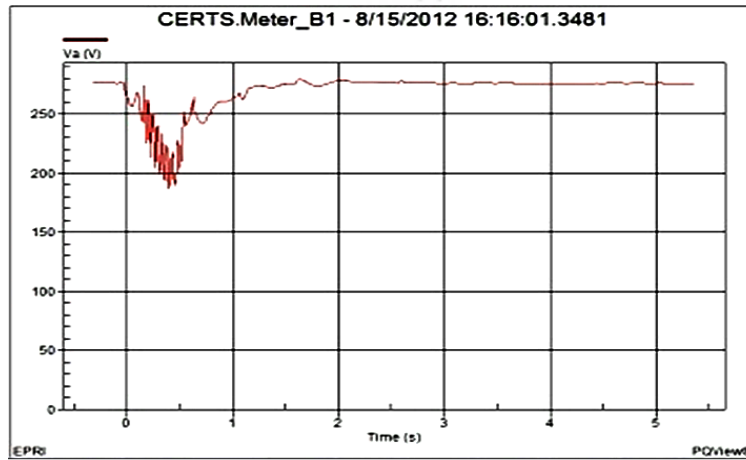
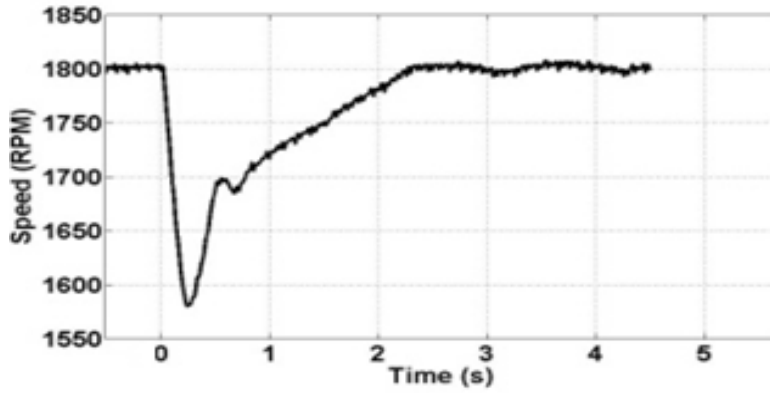


Figure 2.5 Experimental plots showing the genset response with load relief (V/Hz) scheme for a 20–95 kW step change in electrical load

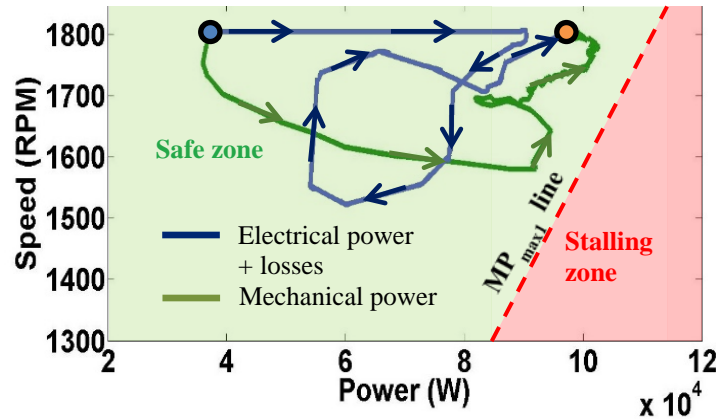


Figure 2.6 Locus of the speed vs. active power characteristics of the genset with load relief (V/Hz) scheme for 20–95 kW step load application

2.4 Prime-mover Stalling in an Inverter-based Distributed Energy Resource

Similar to the gensets (i.e., synchronous generator-based DERs), the inverter-based DERs that have reciprocating engine driven generators as prime-movers also exhibit stalling behavior when they are subjected to large block load changes. However, they present a distinct dynamic response as compared to gensets due to the differences in their operation and controls. Figure 2.7 illustrates the simplified schematic and electromechanical energy conversion process of an inverter-based DER, which can be described by the following energy balance equation [28]:

$$\begin{aligned}
 & \left(\begin{array}{l} \text{Increase in Kinetic} \\ \text{Energy of PMSG, } \Delta KE \end{array} \right) \\
 &= \left(\begin{array}{l} \text{Mechanical Energy} \\ \text{Input to PMSG} \end{array} \right) - \left(\begin{array}{l} \text{Elec. Energy Output} \\ \text{from PCS} \end{array} \right) \\
 & - \left(\begin{array}{l} \text{Total Energy} \\ \text{Dissipated as Losses} \end{array} \right)
 \end{aligned}$$

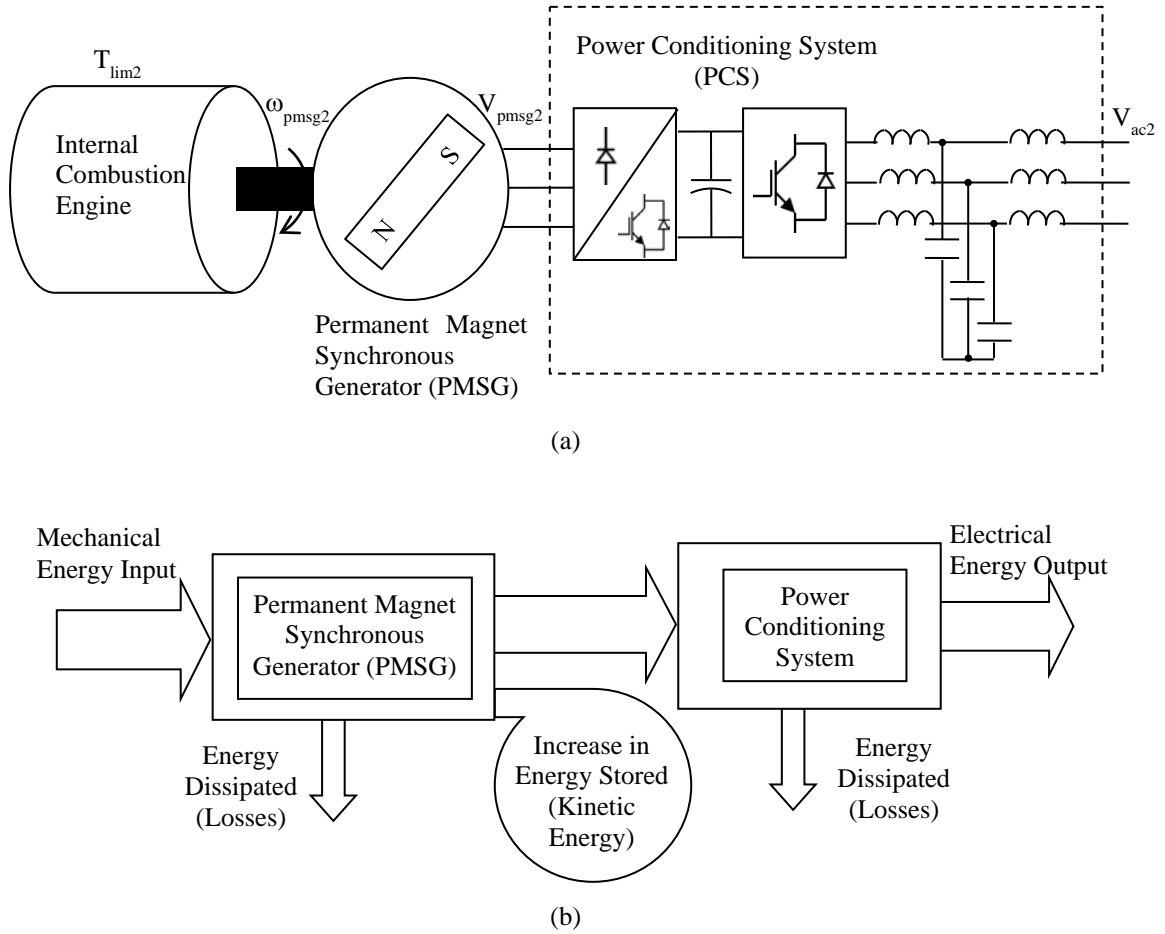


Figure 2.7 An inverter-based distributed energy resource (DER). (a) Simplified schematic, and (b) block diagram of the electromechanical energy conversion process.

The above energy balance equation can be expressed in terms of power quantities as

$$\frac{\Delta KE_2}{\Delta t} = P_{mech2} - P_{elec2} - P_{loss2} \quad (2.12)$$

where P_{mech2} = mechanical power provided by the prime-mover, P_{elec2} = electrical output power of power conditioning system (PCS), and P_{loss2} = total power losses in the permanent magnet synchronous generator (PMSG) and PCS.

Under steady state equilibrium conditions, the left hand side of (2.12).

$$\therefore P_{mech2,ss} = P_{elec2,ss} + P_{loss2,ss} \text{ (in steady state)} \quad (2.13)$$

However, it is possible that the equilibrium condition is not reached after a large load change. This happens because P_{mech2} cannot exceed the rated maximum capability governed by the engine fuel map labeled as MP_{max2} . Hence, the condition for the prime-mover speed to be restored to the steady state equilibrium without stalling is

$$MP_{max2} > P_{elec2} + P_{loss2} \quad (2.14)$$

The above condition for stalling prevention is similar to the case of gensets (cf. (2.5)). However, MP_{max2} varies linearly with the PMSG speed (ω_{pmsg}). In fact, they are related by the constant torque limit of engine fuel map, labeled as T_{lim2} .

$$MP_{max2} = T_{lim2} \cdot \omega_{pmsg2} \quad (2.15)$$

2.4.1 Case study

To gain a deeper understanding of the limiting conditions for prime-mover in inverter-based DER, the case of 0–94 kW step change in electrical load studied earlier (cf. Figure 1.5) is revisited. For this case, the variation of PMSG speed and voltage vs. active power are plotted in Figure 2.8. It was found from experimental testing that the DER’s prime-mover has engine fuel map limit at $T_{lim2} = 398$ Nm, and so the maximum mechanical power from prime-mover (MP_{max2}) varies according to (2.15). Similar to the case of a synchronous generator-based DER [12] — explained in the earlier section — the *Safe* and *Stalling zones* are delineated by the MP_{max2} line [28]. However, a distinguishing characteristic of the inverter-based DER is that the PMSG has no DVR & exciter to regulate its voltage, and therefore the PMSG voltage (i.e., V_{pmsg2} , RMS value) is directly proportional to ω_{pmsg2} as

$$V_{pmsg2} = k_e \cdot \omega_{pmsg2} \quad (2.16)$$

where k_e is the emf constant that was determined from experimental testing as 1.3231 V·s/rad. Hence, the variation of V_{pmsg2} in Figure 2.8 is along the same lines as ω_{pmsg2} (i.e., N_{pmsg2} , when the units are changed from rad./s to rpm).

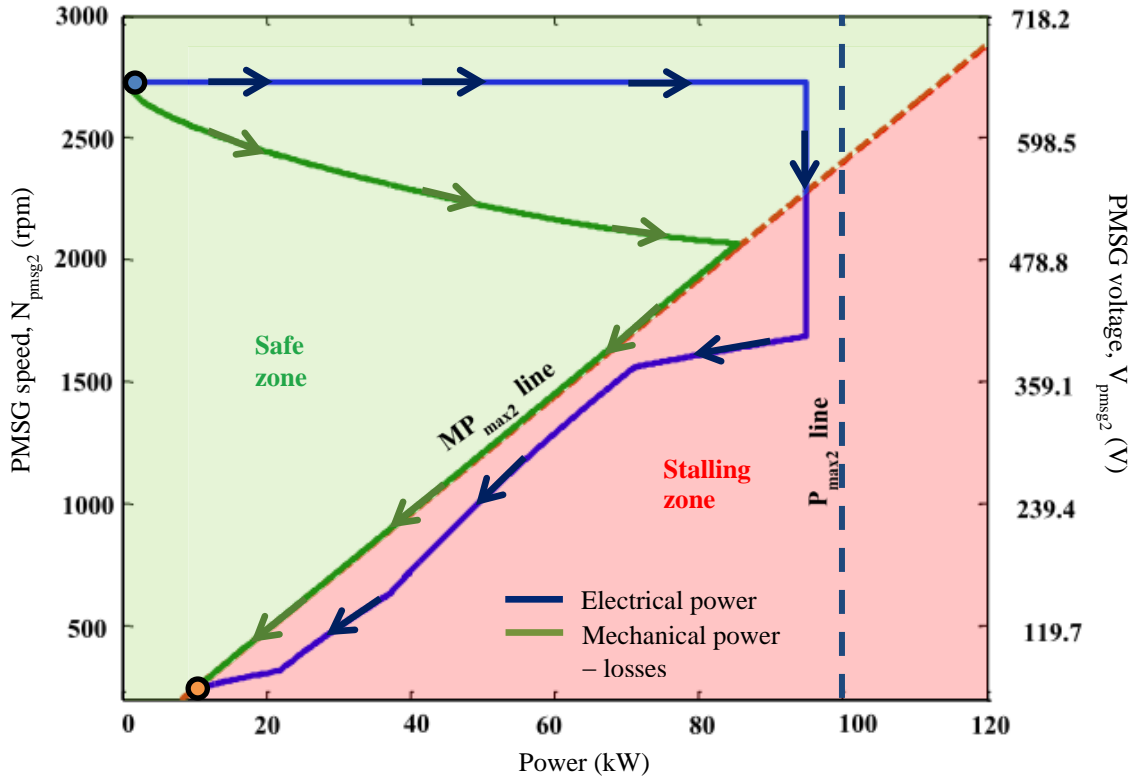


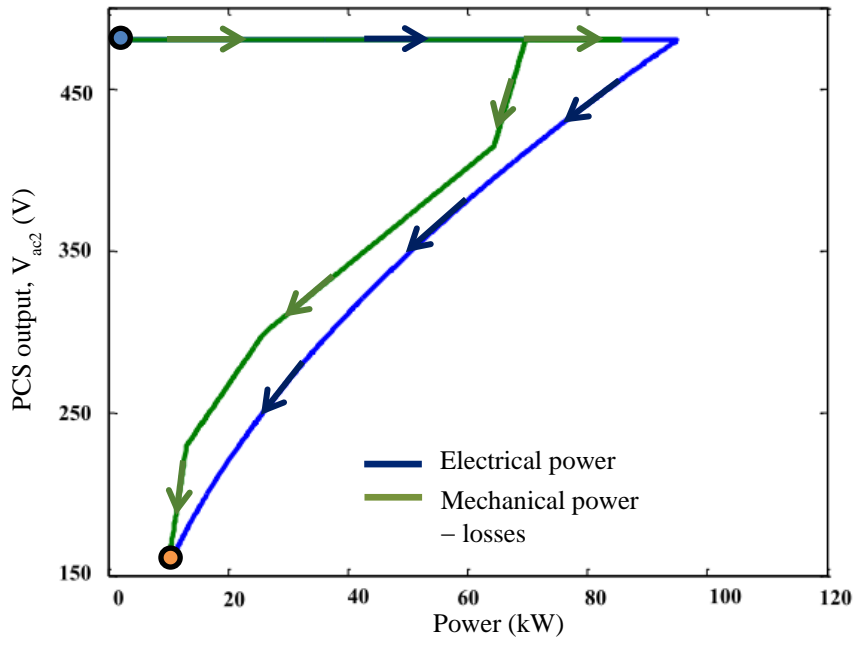
Figure 2.8 Locus of the PMSG speed and voltage vs. active power for the inverter-based DER in response to a 0–94 kW step load application

For the inverter-based DER — similar to the genset covered in the earlier section — the lower limit of PMSG speed that would be restored to equilibrium without stalling is determined from (2.14) and (2.15)

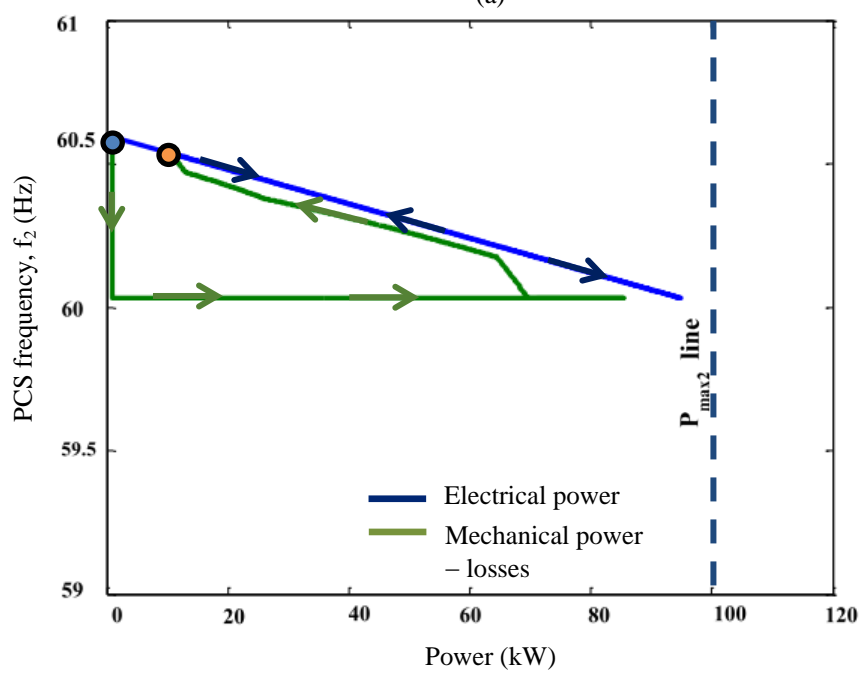
$$N_{L-lim2} [rpm] = \omega_{L-lim2} [rad./s] \times \frac{60}{2\pi} = \frac{P_{elec2}[W] + P_{loss2}[W]}{T_{lim2}[Nm]} \times \frac{60}{2\pi} \quad (2.17)$$

2.4.2 Conditions for prime-mover stalling

The prime-mover stalling occurs when the electrical power trajectory goes into the *Stalling zone* [12]. This is because the mechanical power cannot exceed the rated maximum capability of engine given by the $MP_{\max 2}$ line in Figure 2.10, which illustrates the PMSG speed vs. active power characteristics. However, the additional power conversion system (PCS) stage in the inverter-based DER decouples the output frequency from the PMSG speed. Besides, the PCS output voltage (i.e., V_{ac2} , RMS value) is tightly regulated under normal operations. Nevertheless, when prime-mover stalling occurs, the PCS controls cannot prevent a voltage collapse at the output of inverter-based DER. Therefore, a drop in ω_{pmsg2} or V_{pmsg2} (cf. Figure 2.10) below the threshold would lead to a voltage collapse at the PCS output voltage (i.e., V_{ac2} , RMS value). This is illustrated in Figure 2.9 (a) by the V_{ac2} (RMS value) vs. power characteristics. By contrast, the PMSG speed does not affect the frequency of inverter-based DER shown in Figure 2.9 (b).



(a)



(b)

Figure 2.9 Inverter-based DER output characteristics for a 0–94 kW step load application. (a) PCS output voltage (V_{ac2} , RMS value) vs. active power, and (b) PCS output frequency vs. active power.

Another case when the prime-mover does not stall is shown in Figures 2.11 (a) and (b). In this case, a 0–70 kW step change in load is applied to the terminals of the inverter-based DER. The electrical power trajectory of the prime-mover stayed within the *Safe zone* assuring that the PMSG speed is restored to the steady state equilibrium value without stalling.

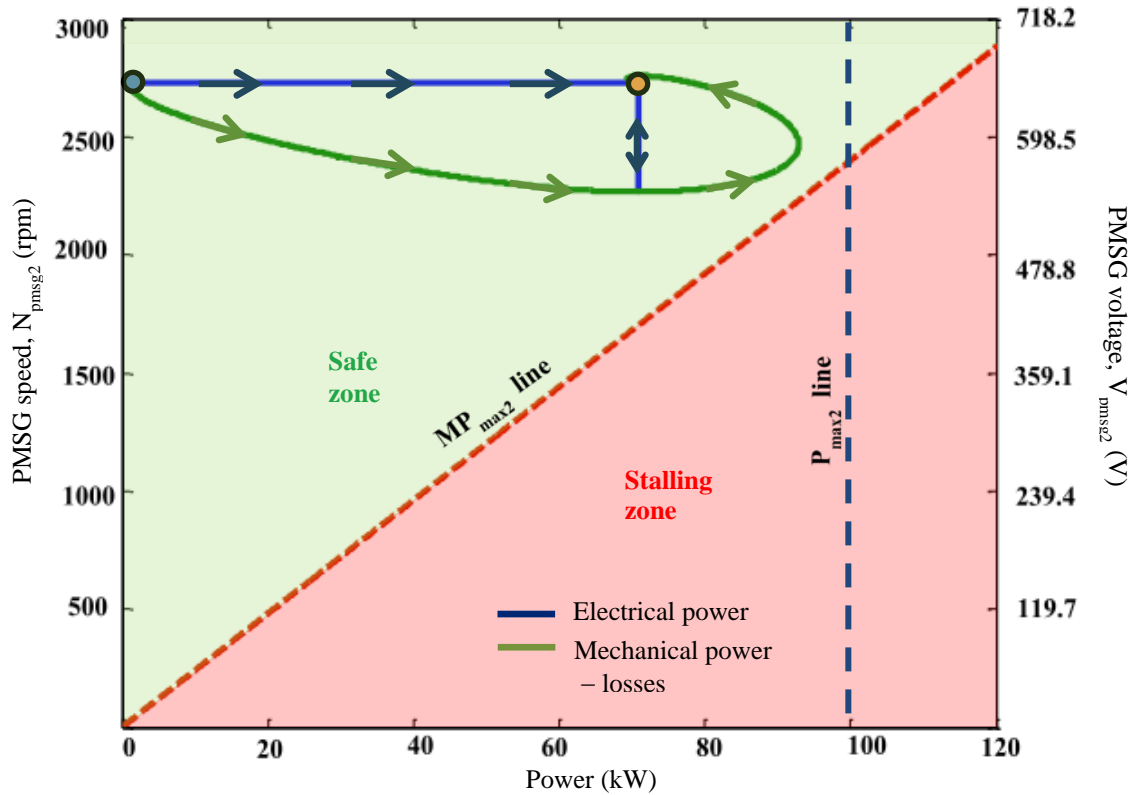
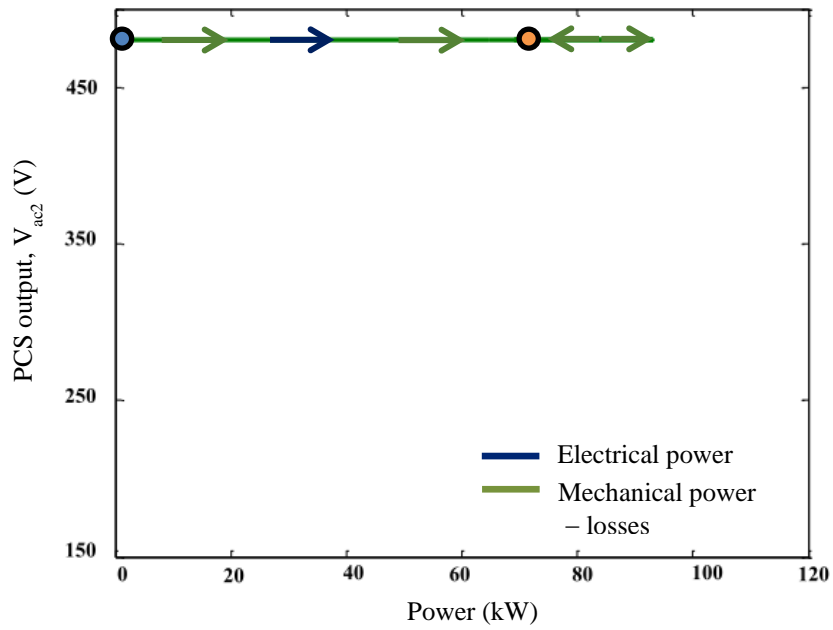
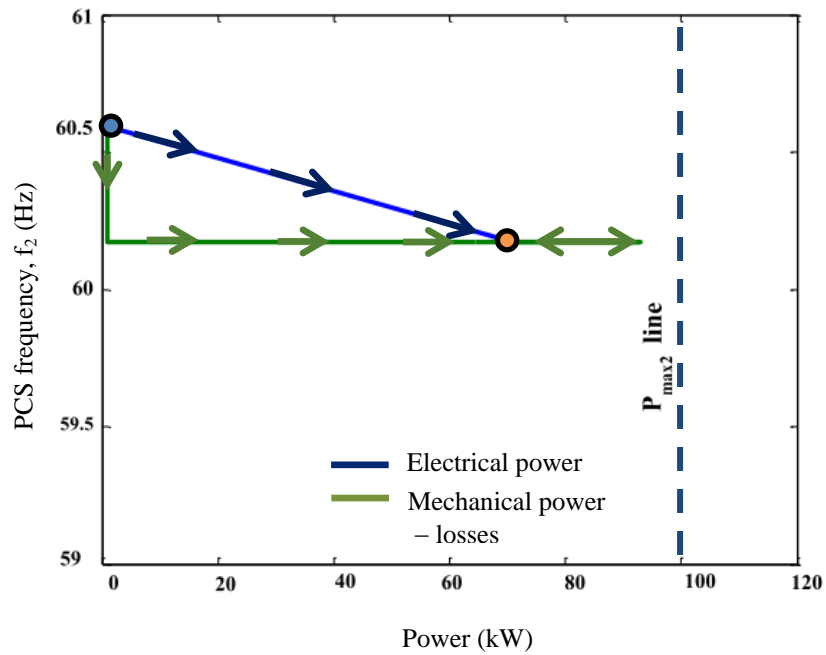


Figure 2.10 Locus of the PMSG speed and voltage vs. active power for the inverter-based DER in response to a 0–70 kW step load application



(a)



(b)

Figure 2.11 Inverter-based DER output characteristics for a 0–70 kW step load application. (a) PCS output voltage (V_{ac2} , RMS value) vs. active power, and (b) PCS output frequency vs. active power.

2.5 Effect of Incremental Load Change on Prime-mover Stalling

The earlier sections covered stalling analysis for both synchronous generator-based and inverter-based DERs. Further case studies for different load changes confirmed that the incremental load change (i.e., ΔP_{elec}) is a key variable affecting the stalling behavior in addition to the final load value [23]. Figure 2.12 illustrates selected results showing the speed restoration to the steady state equilibrium value for small load increments.

Figure 2.12 (a) presents the results of 70–90 kW load change on synchronous generator-based DER, i.e., genset. As seen in this figure, the speed of genset was restored to the steady state equilibrium for 70–90 kW load change [23], [32]. However, the earlier tests showed that the prime-mover would stall for a larger load increment of 0–90 kW.

On similar lines, Figure 2.12 (b) illustrates the results of 60–94 kW load change on inverter-based DER. As seen in this figure, the speed of PMSG (i.e., prime-mover) was restored to the steady state equilibrium for 60–94 kW load change. However, the earlier tests indicated that the prime-mover would stall for a larger load increment of 0–94 kW.

Therefore, it can be concluded from these results that the magnitude of load change, i.e., ΔP_{elec} , is a key variable that influences the prime-mover stalling behavior in both synchronous generator-based and inverter-based DERs. An important takeaway from this analysis is that prime-mover stalling can be avoided by making load changes in smaller increments.

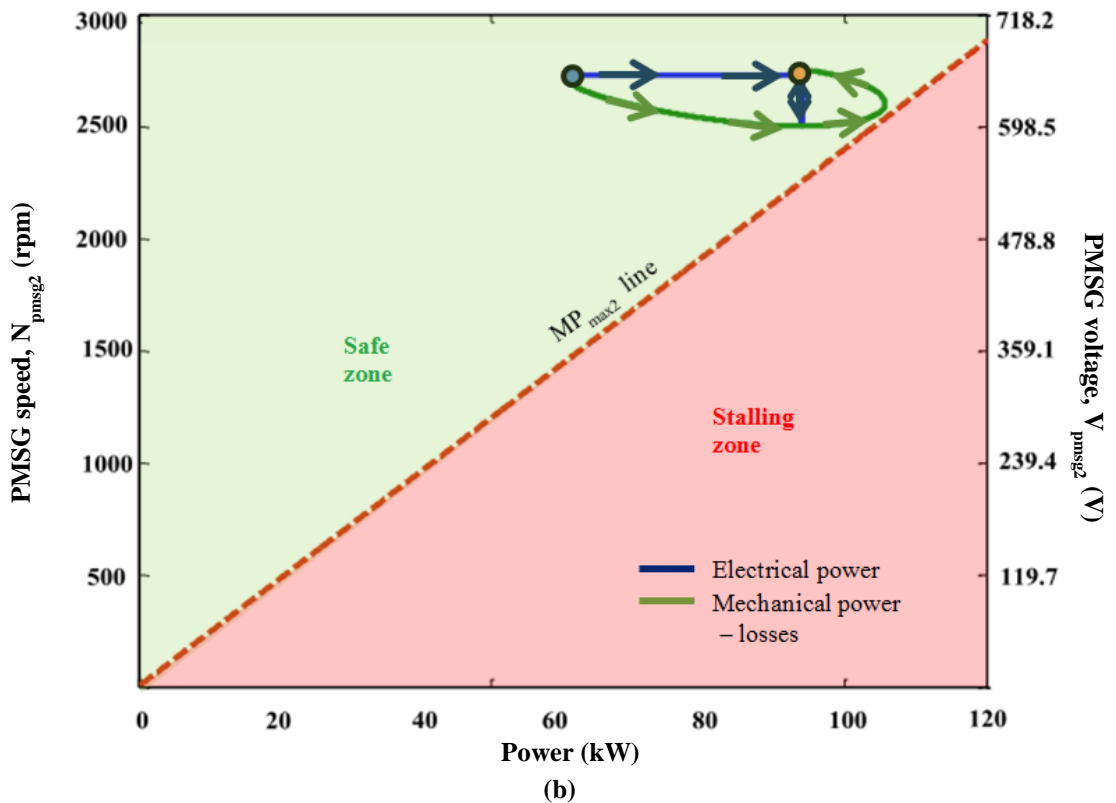
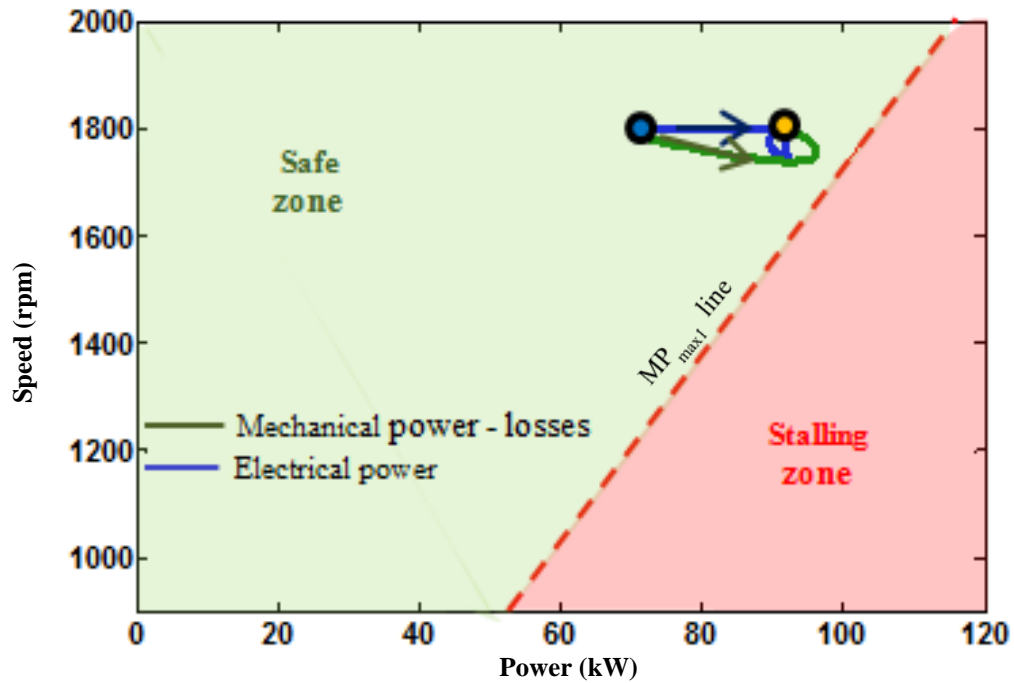


Figure 2.12 Locus of speed vs. active power for (a) genset with 70–90 kW load change, and (b) inverter-based DER with 60–94 kW load change.

2.6 Comparison Between Synchronous Generator-based DERs and Inverter-based DERs

Table 2.2 Synchronous generator-based DERs vs. inverter-based DERs

S. No.	Synchronous generator-based DERs (gensets)	Inverter-based DERs
1	Excellent short circuit handling capacity—due to the large transient reactance of generator	Poor short circuit handling capacity that is limited by the rating of the semiconductor switches employed in PCS
2	Electrical output frequency is directly related to the prime-mover's speed	Electrical output frequency is independent of the prime-mover's speed
3	Can withstand large step changes in load without stalling—due to slow response of controls relative to the inverter-based DERs	More vulnerable to prime-mover stalling since the inverter controls can tightly regulate the terminal voltage to form constant power loads
4	Prime-mover stalling (i.e., speed collapse of the prime-mover) leads to an output frequency collapse	Prime-mover stalling (i.e., speed collapse of the prime-mover) leads to an output voltage collapse
5	Can naturally respond to sudden overloads because of the intrinsic inertia of rotor mass	May require additional surge module (energy storage) to handle large overloads without collapse

2.7 Summary

This chapter presented analysis of the prime-mover stalling in two kinds of natural gas engine powered DERs, viz., synchronous generator-based DER (also known as 'genset') and inverter-based DER. The root cause of stalling behavior is the slow response of primary governor of the reciprocating engine. When a large load change

occurs, the prime-mover speed is lowered temporarily due to the delay in governor response.

At lower speeds, the engine power is derated by the engine fuel map and the mechanical power production of engine is limited by the MP_{\max} line. The engine fuel map limit (MP_{\max} line) is the hardware limit for mechanical power production from engine. Any electrical load demand exceeding the MP_{\max} value would result in prime-mover stalling. Hence, the MP_{\max} line demarcates the boundary between *Safe zone* and *Stalling zone* for DER operation.

When the prime-mover stalls, a genset undergoes a frequency collapse. By contrast, the same condition in an inverter-based DER results in a voltage collapse. This is because the inverter output frequency is decoupled from the prime-mover's speed. The next chapter studies the load sharing operation of synchronous generator-based and inverter-based DERs in an islanded microgrid when limiting conditions are reached in one unit.

CHAPTER 3

DER OPERATION AT LIMITING CONDITIONS IN AN ISLANDED MICROGRID

3.1 Introduction

Earlier chapters presented the modeling and analysis of synchronous generator-based and inverter-based DERs. The distinguishing characteristics and operational vulnerabilities of these two kinds of DERs were outlined. The integration and coordination of these DERs in an islanded microgrid presents new challenges to its survivability. This is especially true when one or more DERs operate near their rated maximum capability in meeting the load demands of microgrid. During a large load change in the islanded microgrid, such DERs are overloaded unless they can off-load the burden to other units with sufficient reserve capacity. When the DERs operate at their limiting conditions, the steady state load sharing is shown to deviate from the active power-frequency (i.e., $P-\omega$) droop curves.

3.2 Load Sharing Between Two Gensets in a Microgrid at Limiting Conditions

In this section, the microgrid performance is analyzed when two interconnected gensets are subjected to large step loads. It is well known that two or more gensets with isochronous governors cannot be connected together as they would ‘fight’ with each

other [33]. Hence, the frequency droop controllers are used to make them all settle at a common steady state frequency based on load sharing between them. The system schematic illustrating connection of the two gensets is shown in Figure 3.1. These two gensets are assumed identical with the ratings and specifications given in Appendix A.

3.2.1 *Case A: Both the gensets are operating in the standalone mode*

At first, the two gensets are operated in the standalone mode with the switch open (cf. Figure 3.1). Their speed governor droop curves are programmed as shown in Figures 3.2 (a) and 3.3 (a), and the load reference setpoints are $P_{ref1} = 0$ kW and $P_{ref2} = 40$ kW. The two gensets are subjected to the same load of 20 – 90 kW. Since the electrical power output (P_{elec}) is higher than the mechanical power (P_{mech}), the stored kinetic energy is expended for energy balance (cf. (2.1)) until the governor responds by increasing P_{mech} . However, the mechanical power production is limited by the engine fuel map to the MP_{max} line as shown in Figures 3.2 (b) and 3.3 (b).

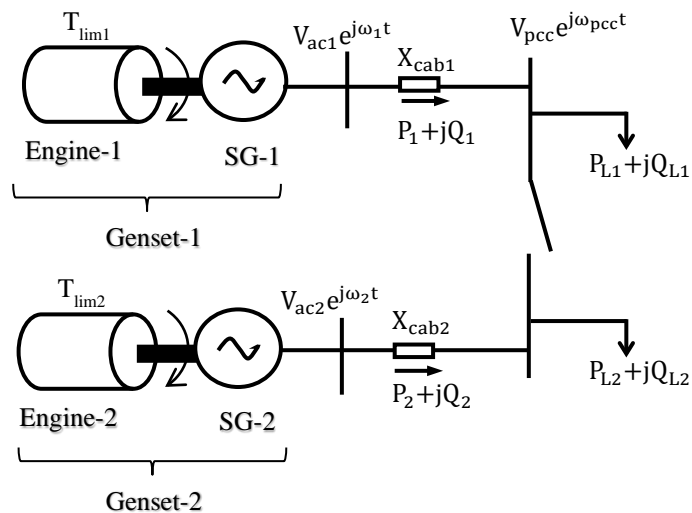
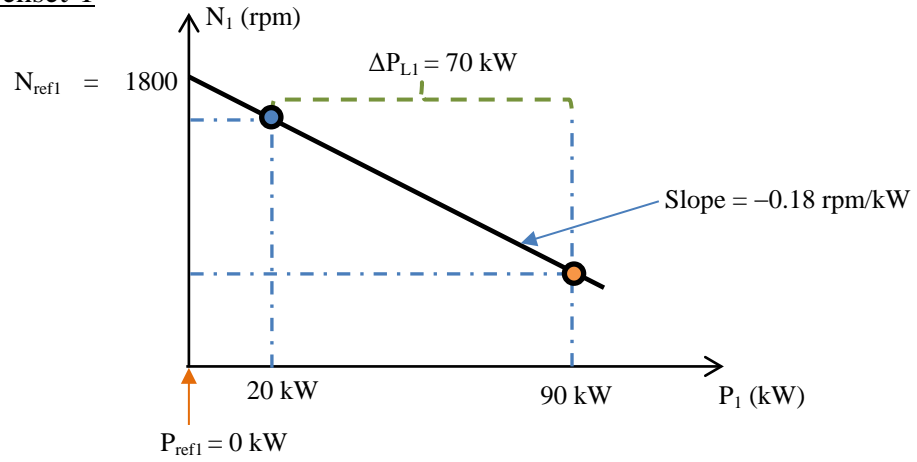
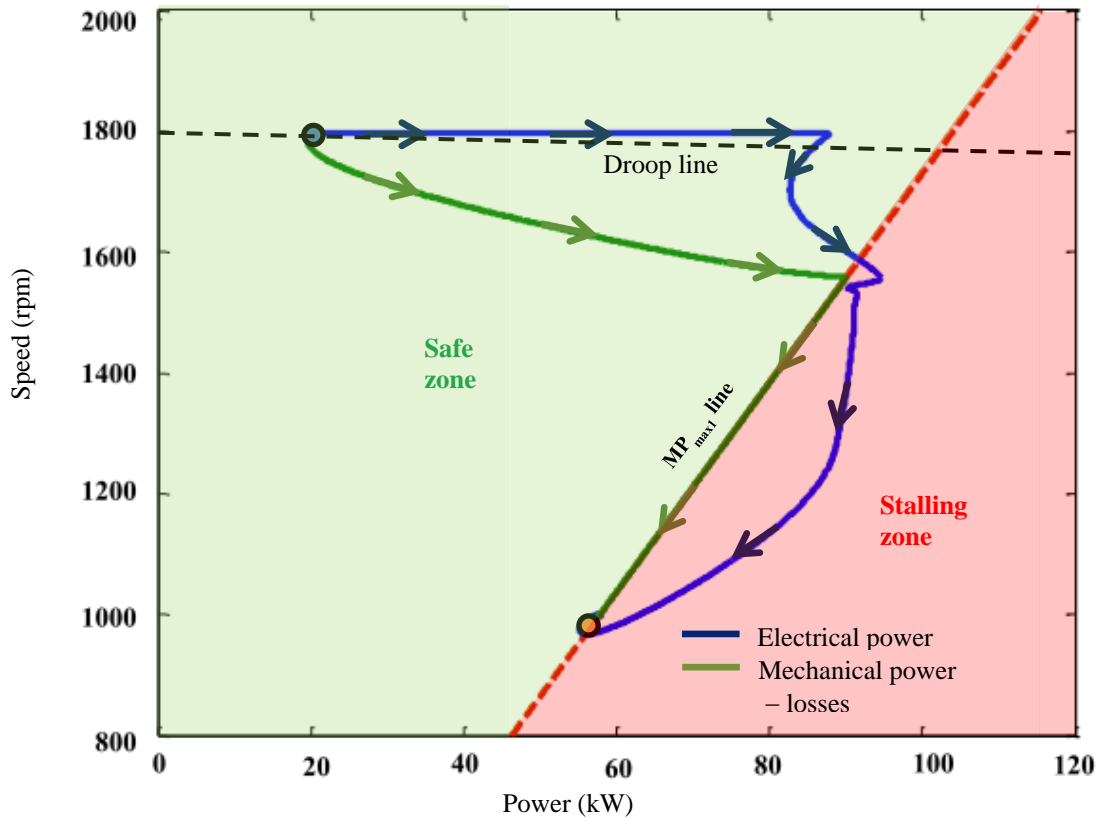


Figure 3.1 Schematic illustrating the interconnection of two gensets in an islanded microgrid

Genset-1



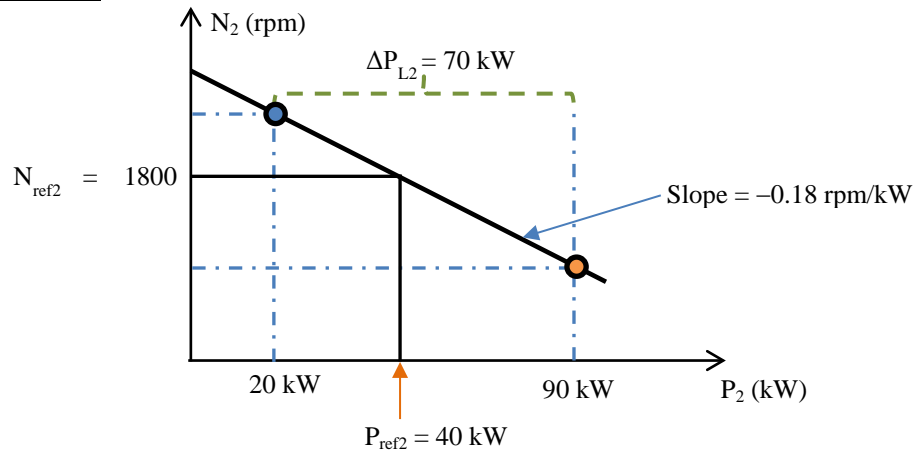
(a)



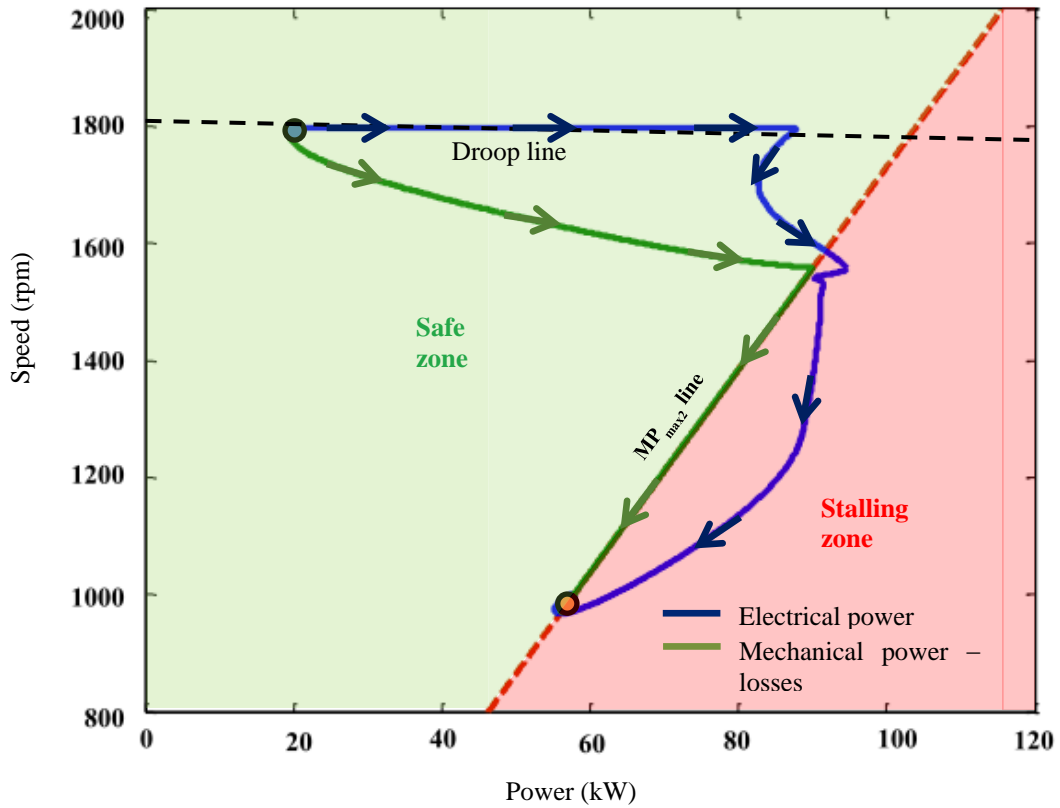
(b)

Figure 3.2 Genset-1 (a) Steady state speed governor droop characteristics with $P_{ref1} = 0$ kW, and (b) locus of the active power-speed response for a 20–90 kW step load application.

Genset-2



(a)



(b)

Figure 3.3 Genset-2 (a) Steady state speed governor droop characteristics with $P_{ref2} = 40$ kW, and (b) locus of the active power-speed response for a 20–90 kW step load application.

The prime-movers of both gensets have stalled because

$$P_{elec1} + P_{loss1} > MP_{max1} \quad (3.1)$$

$$P_{elec2} + P_{loss2} > MP_{max2} \quad (3.2)$$

For both the gensets, the lower limit of generator speed to avoid stalling is determined as

$$N_{L-lim}[rpm] = \frac{90000}{552.0371} * \frac{60}{2\pi} = 1556.95 \text{ rpm} \quad (3.3)$$

In the next case, the two gensets are interconnected by closing the switch.

3.2.2 Case B: Both the gensets are interconnected in a microgrid

In the microgrid, the total load is shared between interconnected gensets as illustrated by the system schematic shown in Figure 3.2. Furthermore, the gensets could help each other by offering additional safety reserves against prime-mover stalling. The underfrequency (V/Hz) scheme is not employed because of the risk of causing large reactive power circulation among the interconnected gensets (cf. Section 3.4).

Here the same load reference setpoints and speed governor droop gains as in Case A are used for the gensets. Moreover, the total load also varies in the same manner from 40 kW to 180 kW. At the beginning, the combined load of 40 kW is shared by both units according to their droop curves. When the two units are running at a steady state speed of 1800 rpm, Genset-2 takes up the entire load of 40 kW since $P_{ref2} = 40 \text{ kW}$ and Genset-1 is not loaded like the pre-load condition in Case A. For Case B, the operation points are indicated by A_1 and A_2 in Figure 3.5, which includes both the steady state load sharing (cf. Figure 3.5 (a)) and the dynamic behavior (cf. Figure 3.5 (b)).

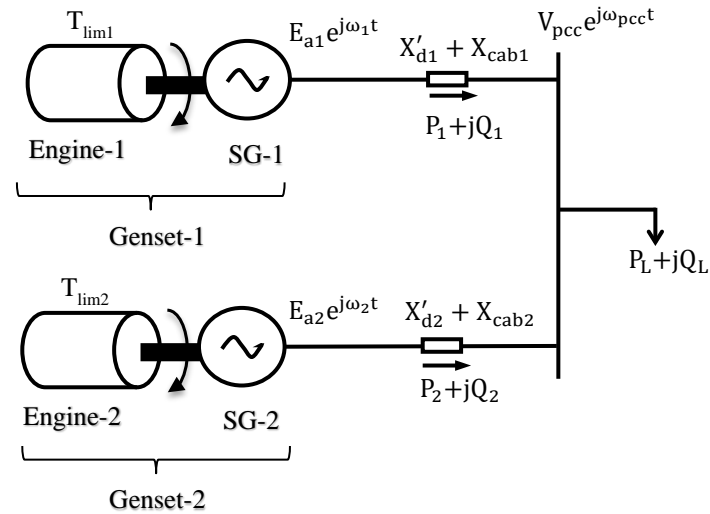


Figure 3.4 Schematic illustrating the interconnection of two gensets in the islanded microgrid. The transient load sharing between gensets is affected by droop gains as well as transient reactances (X'_d).

When the combined load was increased from 40 kW to 180 kW, Genset-2 took a higher proportion of the load than Genset-1. This is indicated by the change in operating points from A_x to B_x (where $x = 1, 2$) in Figure 3.5. It should be noted that at the beginning, the load sharing among gensets is influenced by their respective source reactances and droop gains. Therefore, the synchronous generator is modeled as a back emf (E_a) in series with transient reactance (X'_d) in Figure 3.4.

According to the stalling analysis described in previous chapter, the lower limit of speed for the two gensets — to avoid prime-mover stalling — can be calculated according to the final steady state power allocations [12].

$$N_{L-lim1} = \frac{77000 [W]}{552.0371 [Nm]} \times \frac{60}{2\pi} = 1332 \text{ rpm} \quad (3.4)$$

$$N_{L-lim2} = \frac{103000 [W]}{552.0371 [Nm]} \times \frac{60}{2\pi} = 1782 \text{ rpm} \quad (3.5)$$

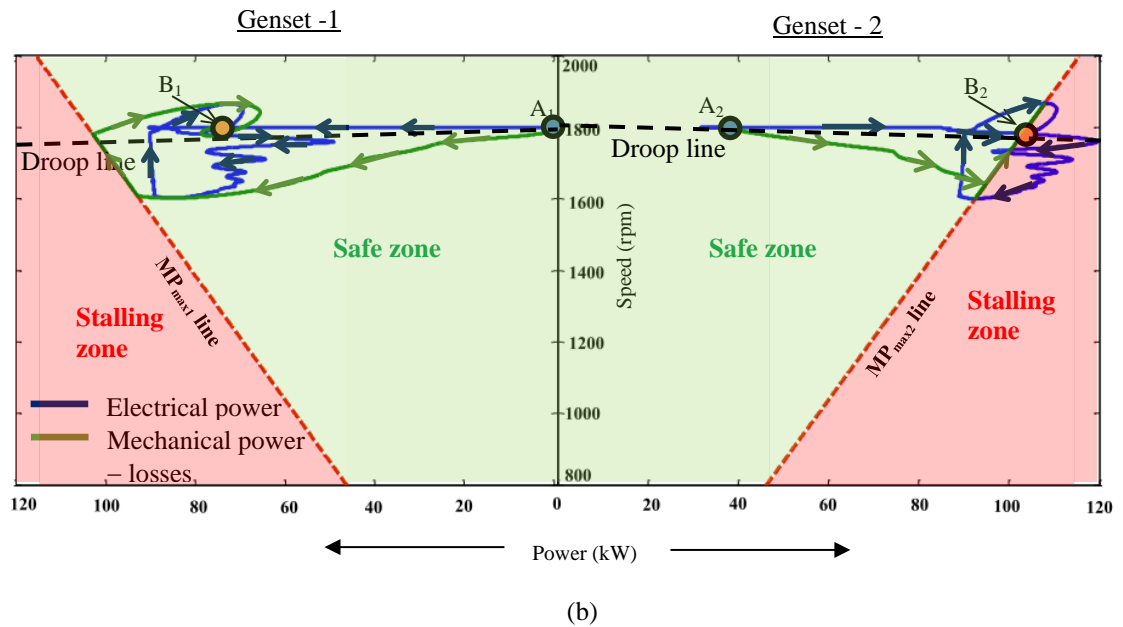
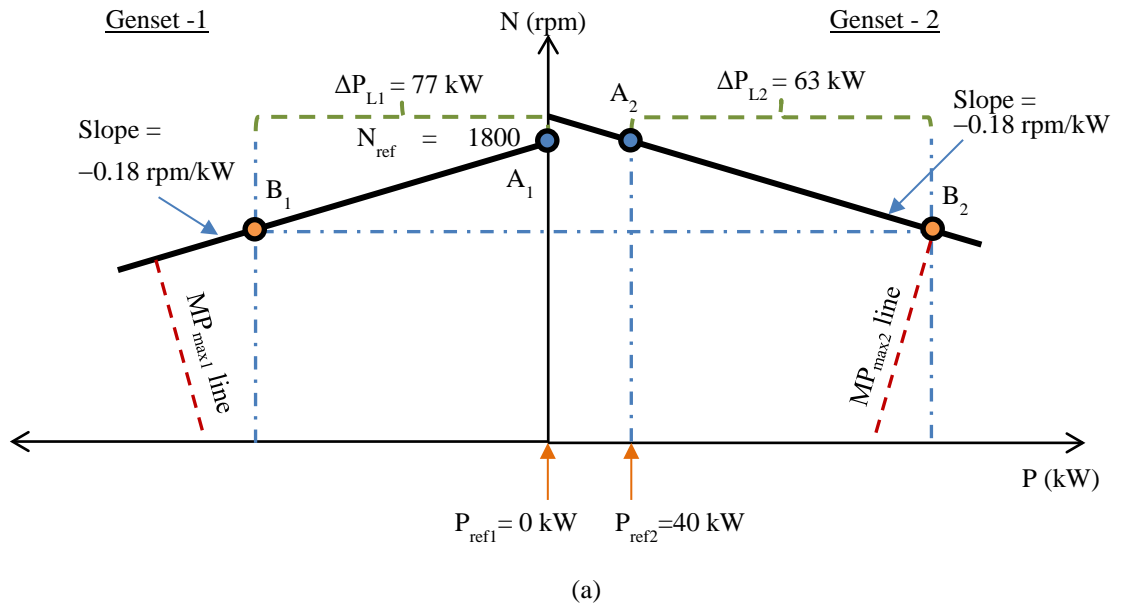


Figure 3.5 Load sharing among Genset-1 and Genset-2. (a) Steady state speed governor droop characteristics, and (b) locus of the active power-speed response for a 40–180 kW step load application.

As seen in Figure 3.5 (b), the speed of Genset-2 has gone below $N_{L\text{-lim}2}$ computed in (3.5). The lower speed operation at $N_2 < N_{L\text{-lim}2}$ should have led to prime-mover stalling in Genset-2. Besides, the dynamic behavior of Genset-2 (cf. Figure 3.5 (b)) also points out that the electrical load shared by it has briefly exceeded the $MP_{\text{max}2}$ line. However, it did not happen because Genset-1 has sufficient safety margin to cover itself and pull out Genset-2 from its *Stalling zone*. This can be observed from Genset-1 response in Figure 3.5 (b) and its $N_{L\text{-lim}1}$ calculation of 1332 rpm in (3.4). Interestingly, the added safety reserve of Genset-1 has protected Genset-2 from stalling (and has extended the *Safe zone*) although Genset-2's speed dropped below its $N_{L\text{-lim}2}$ of 1782 rpm as per (3.5).

3.3 Load Sharing in a Mixed Source Microgrid Under Limiting Conditions

A mixed source microgrid comprises diverse kinds of DERs. The CERTS Microgrid is a mixed source microgrid with synchronous generator-based (i.e., genset) and inverter-based DERs. Studies are carried out to investigate the dynamic behavior of CERTS Microgrid (cf. Figure 1.1), when the DERs are operated at their limiting conditions [14].

3.3.1 Case A: DER-1 (genset)—operated in the isochronous mode; DER-2 (inverter-based DER)—CERTS droop controller setpoints: $P_{\text{ref}2} = 0 \text{ kW}$, $Q_{\text{ref}2} = 0$, $P_{\text{max}2} = 100 \text{ kW}$.

Figure 3.6 shows a simplified schematic of the mixed microgrid under test. As the genset is operated in the isochronous mode, its speed is regulated at the nominal speed.

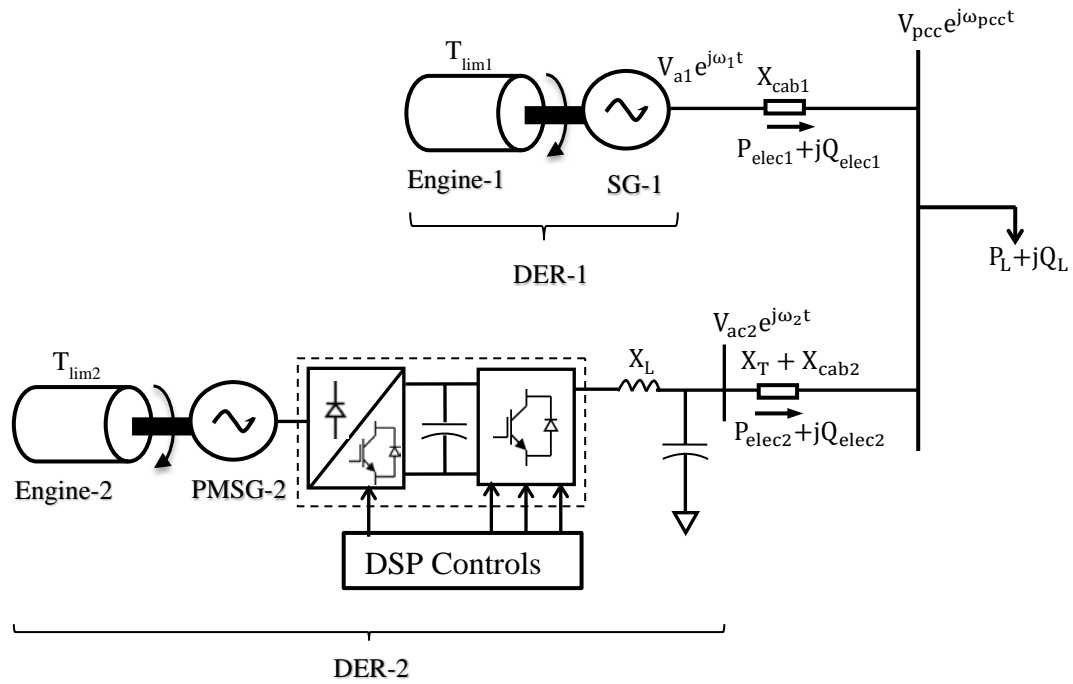


Figure 3.6 Schematic of the mixed source microgrid comprising synchronous generator-based and inverter-based DERs

The aim of this study is to investigate the system dynamic behavior when the genset reaches the engine fuel map limits (i.e., MP_{max1} line).

Simulation results from MATLAB®/Simulink™ illustrating the system performance for 75–150 kW load change are shown in Figure 3.7. The corresponding experimental results from the CERTS Microgrid validating the models are displayed in Figure 3.8. Before the load change, the genset takes up the entire burden of 75 kW since the load reference setpoint on the inverter-based DER, i.e., $P_{ref2} = 0$ kW. At the instant of the load change event, the inverter-based DER experienced the major transient burden. This is due to its lower output reactance ($X_L + X_T = 0.06$ p.u.) as compared to the transient reactance of generator ($X'_d = 0.184$ p.u.) [34]. However, it should be noted that there is discrepancy

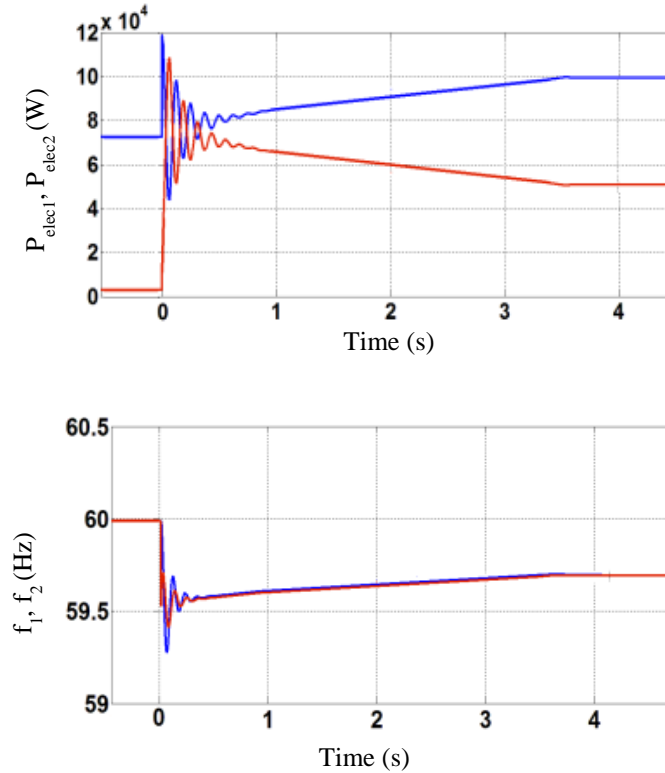


Figure 3.7 Simulation results illustrating the system performance for a load change from 75 kW to 150 kW. DER-1 (genset in blue): isochronous governor; DER-2 (inverter-based DER in red): $P_{ref2} = 0$ kW, $P_{max2} = 100$ kW.

in terms of damping between the simulation results and experimental data. It is attributed to lack of complete details in the published information on commercially manufactured DERs.

On the other hand, the steady state frequency after the load change event is not restored to the nominal value by the genset's isochronous governor. This is because the genset's output increased to take up the extra burden since the inverter's load reference setpoint (P_{ref2}) is 0 kW. However, the genset's mechanical power production got limited by the engine fuel map to around 100 kW @ 59.7 Hz. Therefore, the remaining load of

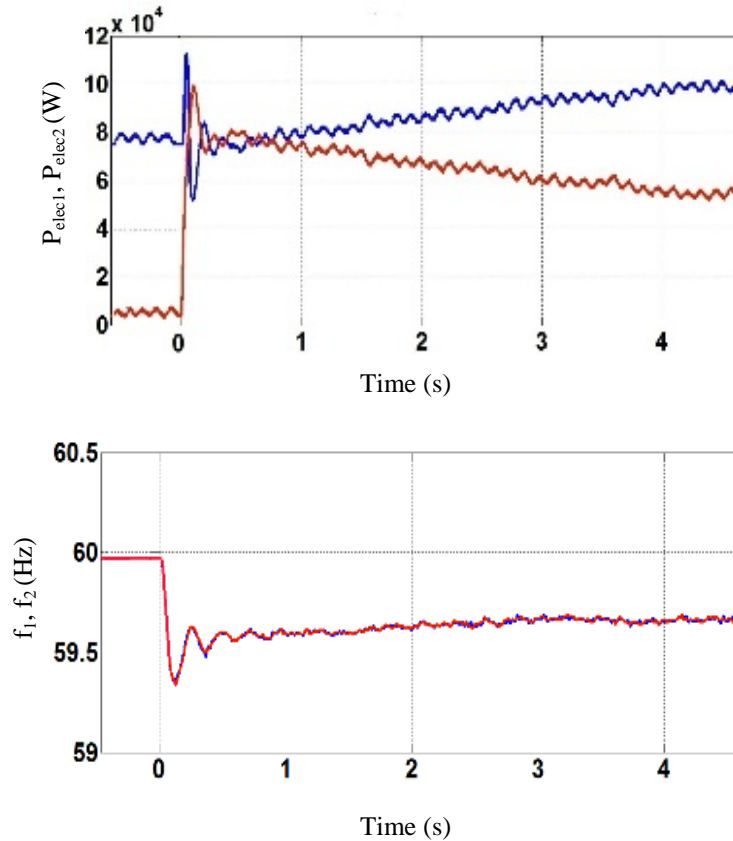


Figure 3.8 Experimental results illustrating the system performance for a load change from 75 kW to 150 kW. DER-1 (genset in blue): isochronous governor; DER-2 (inverter-based DER in red): $P_{ref2} = 0$ kW, $P_{max2} = 100$ kW.

50 kW is transferred to the inverter-based DER (despite having $P_{ref2} = 0$) and the frequency dropped according to the droop gain programmed in its controller.

The steady state behavior can be better explained by the graphical illustration in Figure 3.9. As seen in this figure, the genset got limited by its fuel map (i.e., MP_{max1} line) to take just 25 kW more load burden. Therefore, the inverter-based DER is forced to take up the balance load of 50 kW. During this action, the system cannot bring the steady state

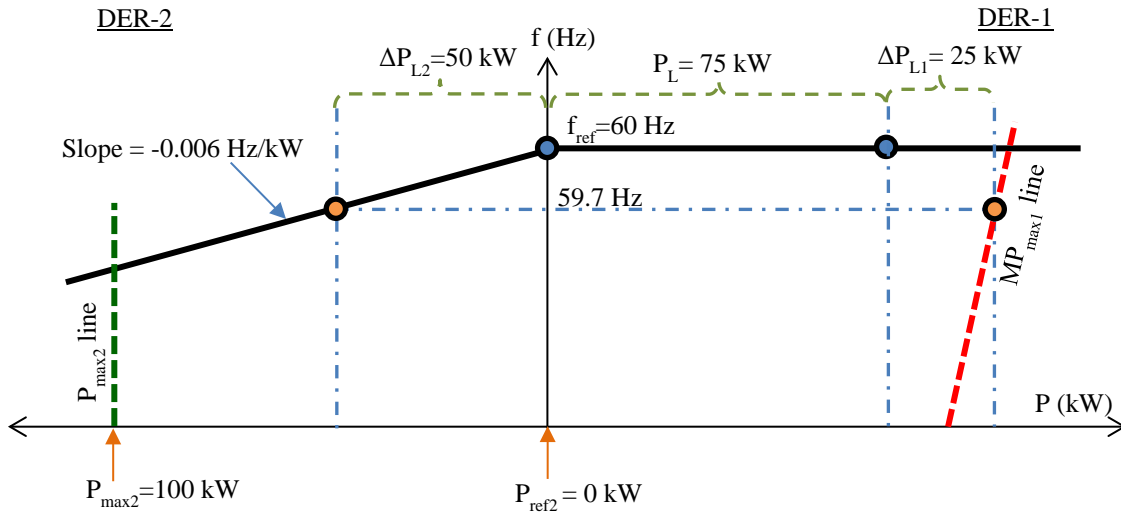


Figure 3.9 Steady state load sharing between DER-1 and DER-2 for a load change from 75 kW to 150 kW. DER-1 (genset): isochronous governor; DER-2 (inverter-based DER): $P_{ref2} = 0$ kW, $P_{max2} = 100$ kW.

frequency back to its nominal value of 60 Hz — despite having an isochronous governor for controlling the genset.

3.3.2 Case B: DER-1 (genset)—CERTS droop controller setpoints: $P_{ref-1} = 80$ kW, $Q_{ref-1} = 0$, $P_{max-1} = 93$ kW; DER-2 (inverter-based DER)—CERTS droop controller setpoints: $P_{ref-2} = 0$ kW, $Q_{ref-2} = 0$, $P_{max-2} = 100$ kW.

In this study, both the genset and inverter-based DER are programmed with the CERTS controls, i.e., P- ω droop controller and P_{max} controller (cf. Figures 1.2 and 1.3). Under normal operation, the P- ω droop characteristics decide the steady state load sharing between the two DERs. However, the limiting conditions may apply for large load changes. The load sharing is affected by either the engine fuel map limit (i.e., MP_{max} line) or the programmed CERTS P_{max} value, whichever is lower [14].

The simulation results from MATLAB®/Simulink™ and experimental data showing the behavior of the DERs when the load is increased from 75–150 kW are illustrated in Figures 3.10 and 3.11, respectively. At first, for the 75 kW load condition the genset (i.e., DER-1) is dispatched at 75 kW and inverter-based DER at 0 kW — as the load reference setpoints programmed at $P_{ref1} = 75$ kW and $P_{ref2} = 0$ kW. When the load is increased from 75 kW to 150 kW, the genset (DER-1) load sharing is limited by its CERTS maximum power controller value, which was programmed as $P_{max1} = 93$ kW. Moreover,

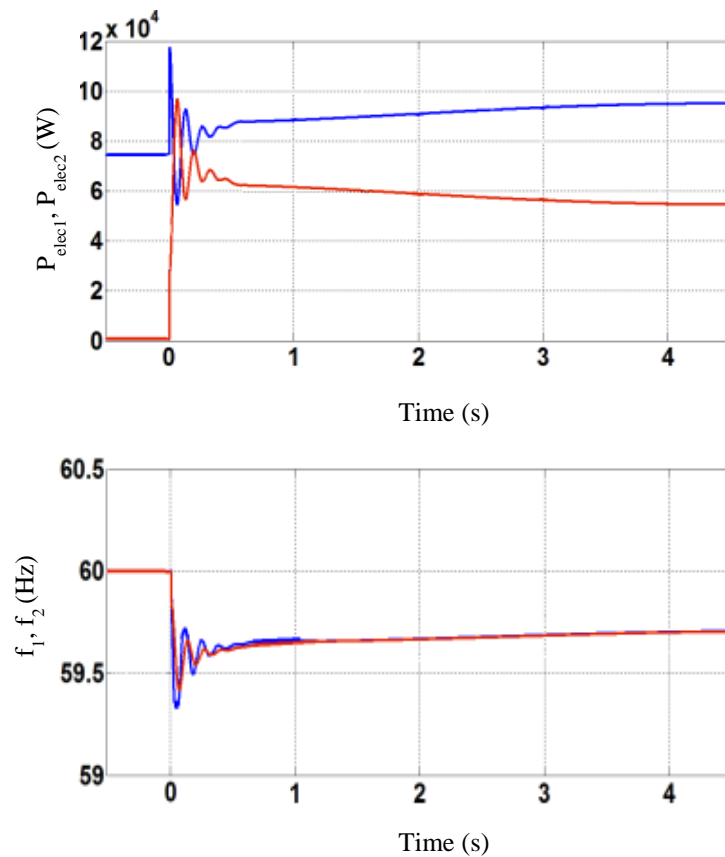


Figure 3.10 Simulation results illustrating the system performance for a load change from 75 kW to 150 kW. DER-1 (genset in blue): $P_{ref1} = 75$ kW, $P_{max1} = 93$ kW; DER-2 (inverter-based DER in red): $P_{ref2} = 0$ kW, $P_{max2} = 100$ kW.

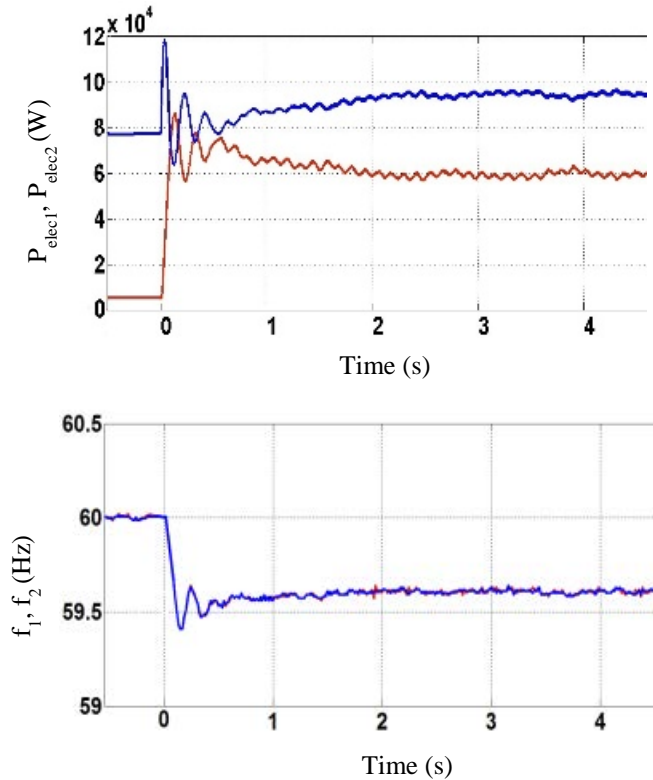


Figure 3.11 Experimental results illustrating the system performance for a load change from 75 kW to 150 kW. DER-1 (genset in blue): $P_{ref1} = 75$ kW, $P_{max1} = 93$ kW; DER-2 (inverter-based DER in red): $P_{ref2} = 0$ kW, $P_{max2} = 100$ kW.

the steady state frequency is no more dictated by the droop curves. This can be observed from the graphical illustration in Figure 3.12.

As seen in Figure 3.12, when the load is increased from 75 kW to 150 kW, the genset output got limited by its P_{max1} value to just an additional 18 kW. Hence, the other DER in the microgrid (i.e., inverter-based DER) is forced to take up the balance load of 57 kW. During this action, the system deviated from the droop curves and settled at the steady state frequency of 59.66 Hz.

Thus, the CERTS controls offer the software flexibility in setting the maximum power (i.e., P_{max1}) through programming to any value less than the engine fuel map limit

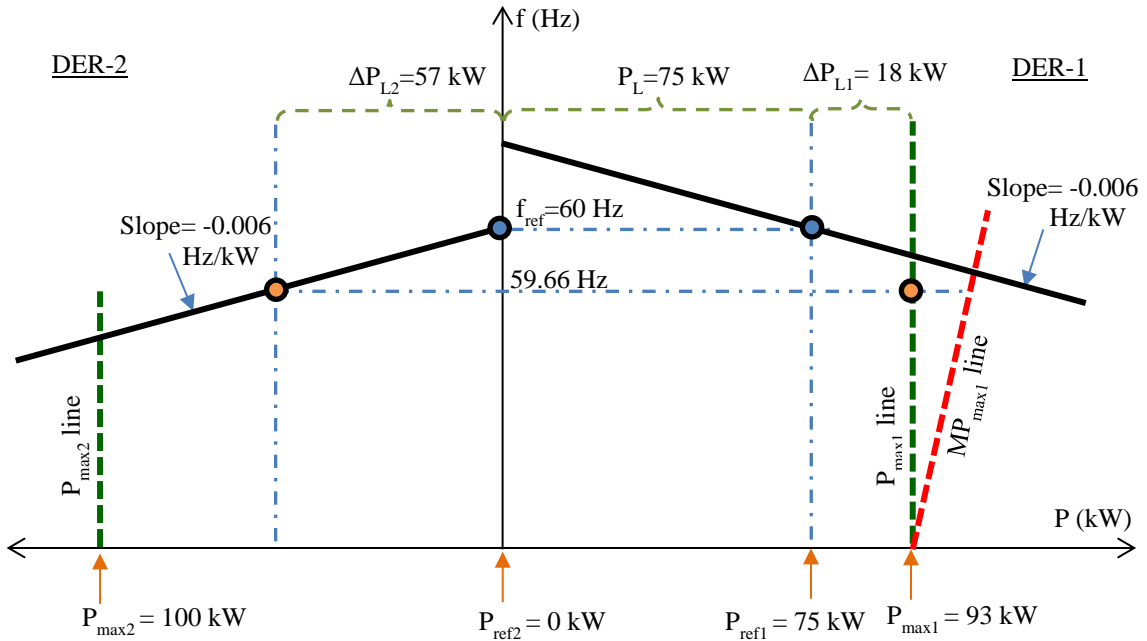


Figure 3.12 Steady state load sharing between DER-1 and DER-2 for a load change from 75 kW to 150 kW. DER-1 (genset): isochronous governor; DER-2 (inverter-based DER): $P_{ref2} = 0$ kW, $P_{max2} = 100$ kW.

(i.e., MP_{max} line) [14]. Therefore, one of the key advantages in using such controls is that even a smaller rated synchronous generator can be driven from the same prime-mover by programming a lower value $P_{max} < MP_{max}$. Otherwise, the generator would need to be oversized above the engine rated maximum capability (i.e., MP_{max}), as seen in the earlier case of the isochronous governor controlled genset.

3.4 Why is the Underfrequency Load Relief (V/Hz) Scheme not used in Gensets for Operation in Microgrid?

It was observed earlier in Section 2.3 that the underfrequency load relief (V/Hz) scheme could prevent the prime-mover stalling condition in gensets for standalone mode of operation. This is because the V/Hz scheme senses a decrease in frequency below a

threshold value and proportionately lowers the voltage reference to the DVR/exciter of the genset. Then the reduced voltage applied to the load is expected to lower its power demand. Thus, the power drawn by the load can be lowered below the rated maximum capability of engine.

However, when the genset is interconnected with an inverter-based DER — in a mixed source microgrid (cf. previous section) — the lowering of genset voltage may be detrimental to the microgrid. The simulation results illustrating the dynamic behavior of DERs when the load in the mixed source microgrid is increased 75–150 kW are shown in Figure 3.13. As seen in this figure, when the load relief (V/Hz) scheme is employed in the genset alone, its voltage was reduced below that of inverter-based DER. Even though the difference between the voltages of two DERs is small, it caused a large reactive power circulation between them.

In the CERTS Microgrid, the Marathon Electric’s DVR2000E was installed at first to regulate the terminal voltage of the genset. However, it was found to be constraining the load relief to a minimum non-zero value (and not allow programming ‘0’ V/Hz). Hence, it was replaced with Basler’s DECS-250 DVR in the experiments conducted later. The purpose of disabling the load relief scheme (by programming ‘0’ V/Hz) is to prevent reactive power circulation between gensets in the microgrid.

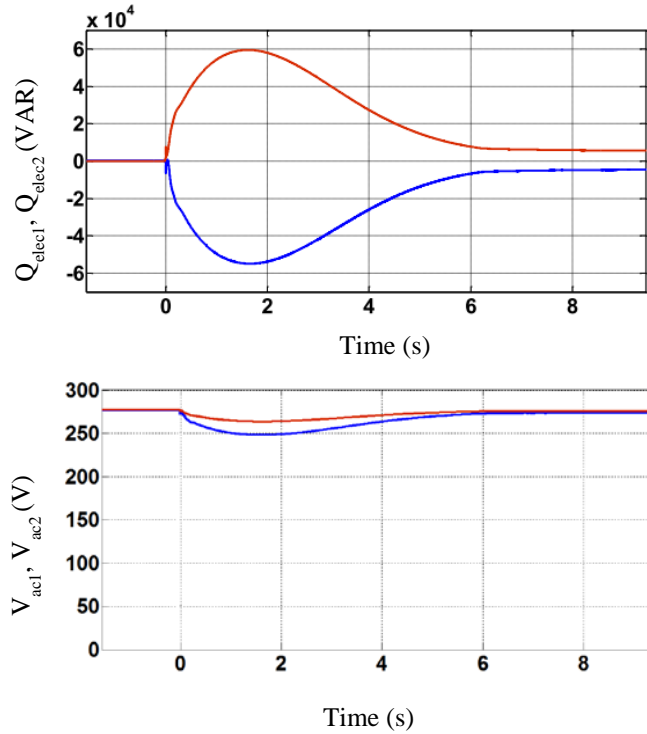


Figure 3.13 Experimental results illustrating the system performance for a load change from 75 kW to 150 kW. DER-1 (genset in blue): $P_{ref1} = 0$ kW, $P_{max1} = 100$ kW, and load relief (V/Hz) is enabled; DER-2 (inverter-based DER in red): $P_{ref2} = 0.75$ kW, $P_{max2} = 100$ kW.

3.5 Summary

This chapter presented the load sharing between interconnected DERs when they reached limiting conditions in an islanded microgrid. It was shown that interconnected DERs could aid each other by providing added safety reserve to the engine fuel map limits (MP_{max} line). Furthermore, CERTS P_{max} controls offer flexibility to limit the DER power output to within the engine rated maximum capability. While the engine fuel map limit (MP_{max} line) is the hardware limit for engine mechanical power, the CERTS P_{max} value can be programmed in the control software to limit the electrical power output.

CHAPTER 4

CONTROL AND PREVENTION OF PRIME-MOVER STALLING IN DISTRIBUTED ENERGY RESOURCES

4.1 Introduction

The earlier chapters discussed the operation and performance of an islanded microgrid when the DERs reach the rated maximum capability. It was observed that synchronous generator-based DERs (i.e., gensets) interconnected in a microgrid aided each other against prime-mover stalling by augmenting their margin capacity reserves (cf. Section 3.2). Similar trend took place in a mixed source microgrid where an inverter-based DER with enough reserve capacity came to the assistance of a genset that reached its limiting condition (cf. Section 3.3). However, during experiments carried out at the CERTS Microgrid, the results were negative when the power allocations of genset and inverter-based DER were equal [28]. The inverter-based DER could not be prevented from stalling upon load increase by an interconnected genset sharing the load equally. Therefore, further investigations are carried out to understand the impact of sluggish genset controls vis-à-vis fast inverter controls on the system dynamic behavior. Various control strategies are studied to avoid prime-mover stalling condition in gensets as well as inverter-based DERs [28].

4.2 Analysis of DER Prime-mover Stalling in a Mixed Source Microgrid

The mixed source microgrid comprising both genset and inverter-based DER is reexamined in this section for more severe conditions than before (cf. Section 3.3), but which could result in prime-mover stalling. Figure 4.1 gives a simplified circuit schematic of the system under investigation. The dynamic modeling and simulation was carried out in MATLAB®/Simulink™ using SimPowerSystems toolbox. It is assumed that the genset is controlled by an isochronous governor, whereas the controls for inverter-based DER are the same as in Figure 1.4. To validate the simulation models, experimental test data from CERTS Microgrid was used. However, it should be noted

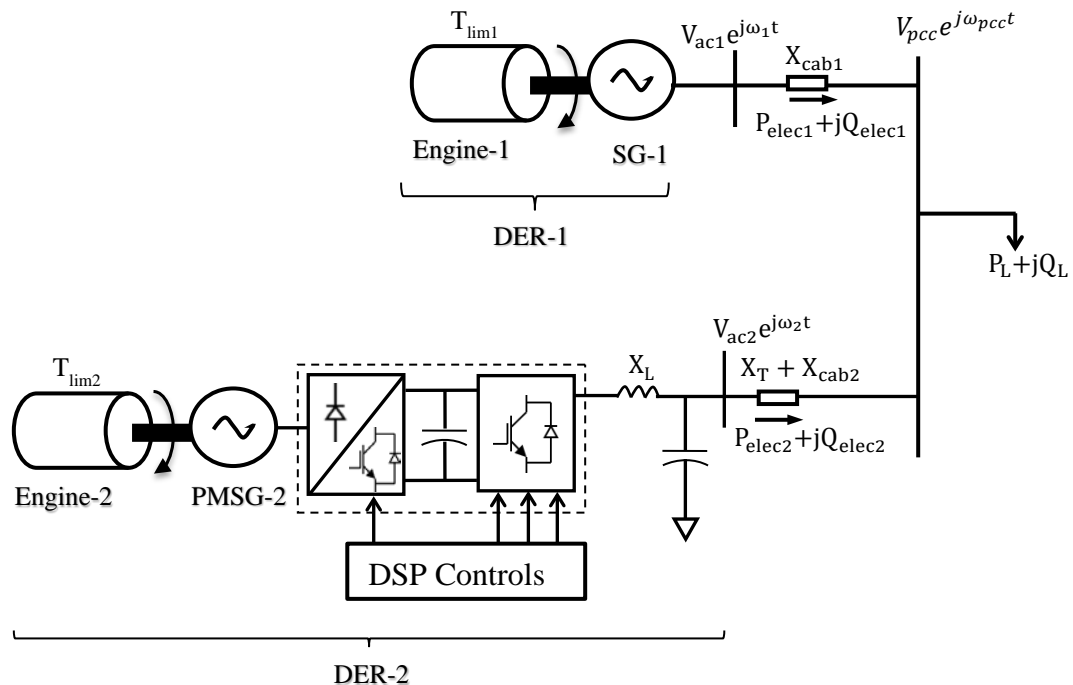


Figure 4.1 Schematic of the mixed source microgrid comprising inverter- and synchronous generator-based DERs.

that the commercial DER equipment do not provide access to all internal state variables. Besides, the data acquisition system was found to have low resolution and quality for some of the measurements. In such instances, the study relies on model-derived quantities for gaining a better understanding of the internal dynamics.

4.2.1 *Case study*

The mixed source microgrid in Figure 4.1 is subjected to a 75–150 kW load change with the genset is running with the isochronous governor, and the load reference setpoint of inverter-based DER at $P_{\text{ref}2} = 37.5$ kW. Figures 4.2 and 4.3 present the experimental waveforms and simulation results for this test. Before the load change event, the original load of 75 kW is equally split between the two DERs. When another 75 kW load is added to the system, the inverter-based DER took the big hit at first — due to its smaller output reactance as compared to the transient reactance X'_d of generator. The sequence of events that took place during this test are illustrated Figures 4.2–4.4. Since the genset is run with an isochronous governor, it is expected become the slack unit and bring the inverter-based DER back to $P_{\text{ref}2} = 37.5$ kW in the steady state. However, as seen in experimental test and computer simulation, the transient load burden on inverter-based DER has tripped it leading to the genset overload and eventually system collapse.

4.2.2 *Discussion of the Microgrid System Collapse*

To examine the sequence of events ①–⑥ in Figures 4.2–4.4, the internal state variables (of inverter-based DER) — not accessible in the commercial unit installed at the CERTS Microgrid test bed — are acquired from the developed model to plot the PMSG speed vs. power presented in Figure 4.5 [28]. From this figure, it is evident that

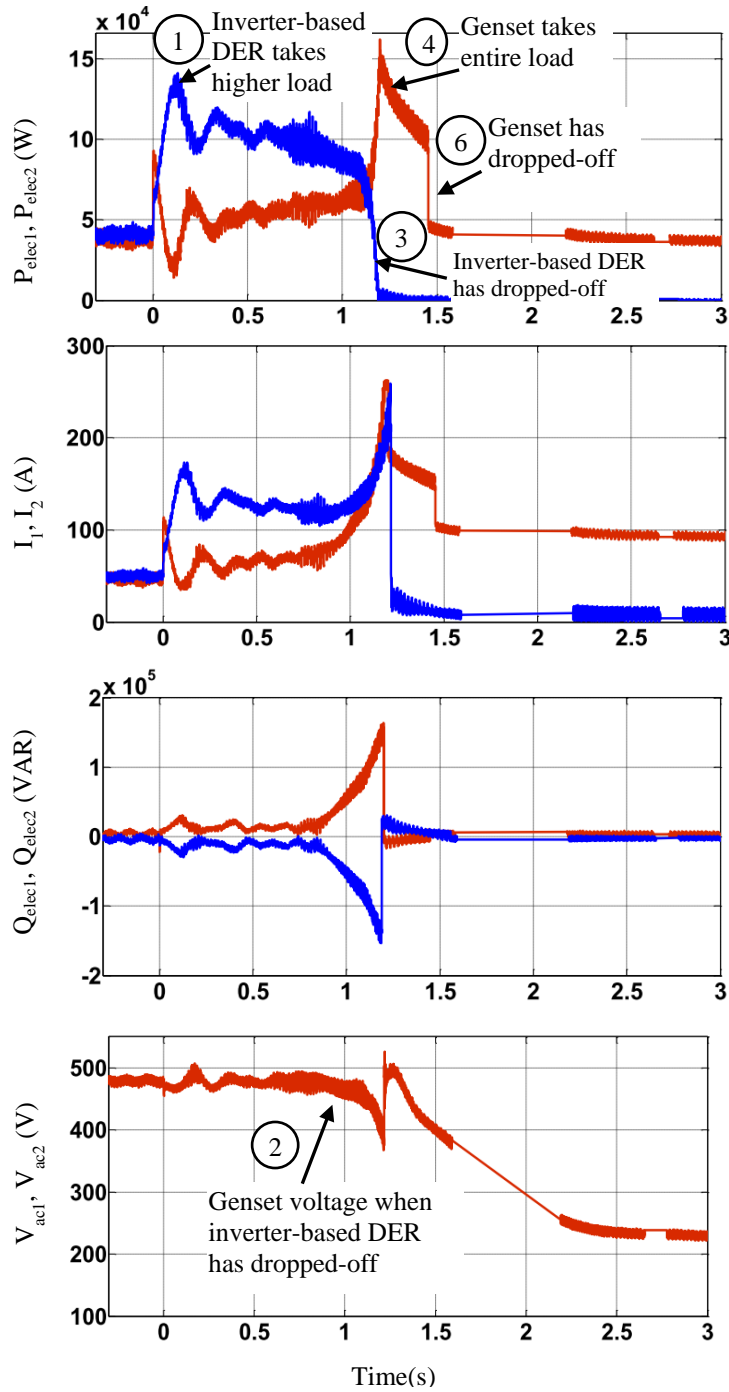


Figure 4.2 Experimental results showing the performance of the DERs for a load change from 75 kW to 150 kW. DER-1 (genset in red): isochronous governor; DER-2 (inverter-based DER in blue): $P_{ref2} = 37.5$ kW, $P_{max2} = 100$ kW.

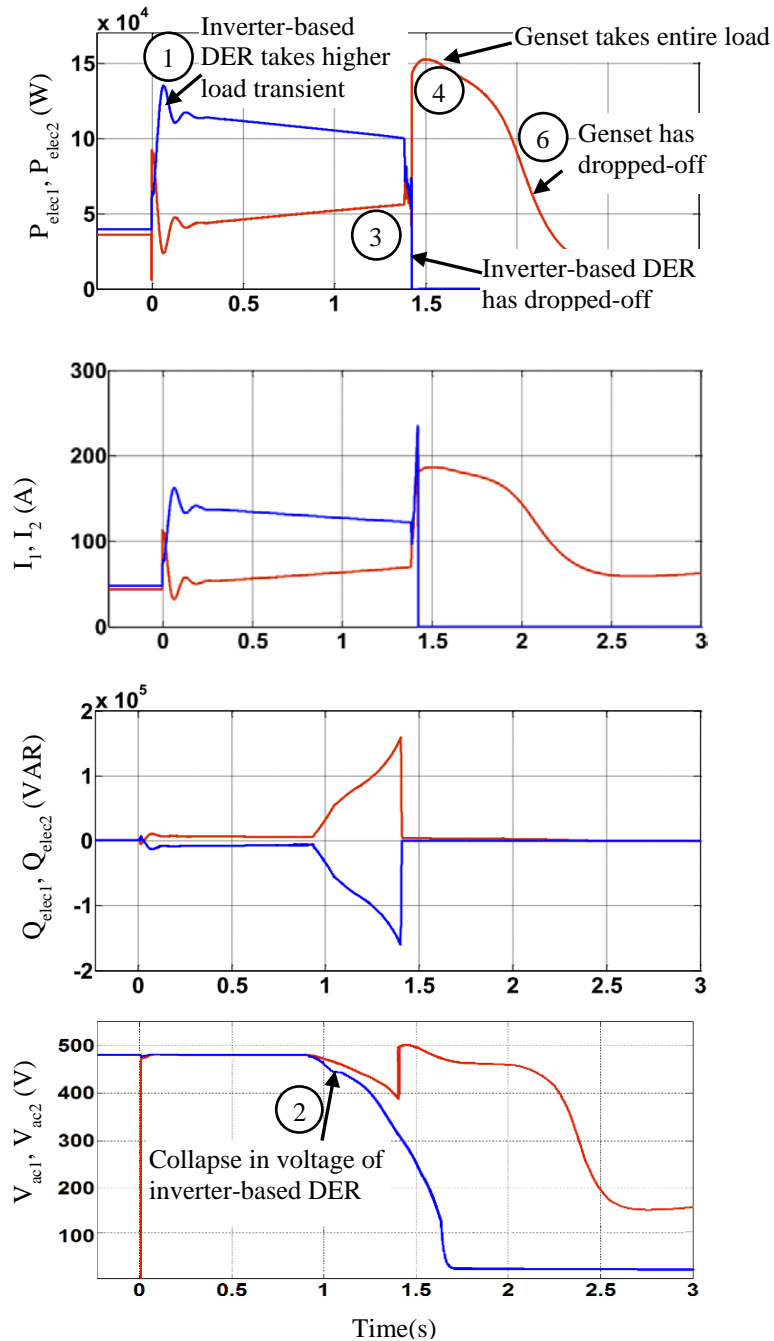


Figure 4.3 Simulation results showing the performance of the DERs for a load change from 75 kW to 150 kW. DER-1 (genset in red): isochronous governor; DER-2 (inverter-based DER in blue): $P_{ref2} = 37.5$ kW, $P_{max2} = 100$ kW.

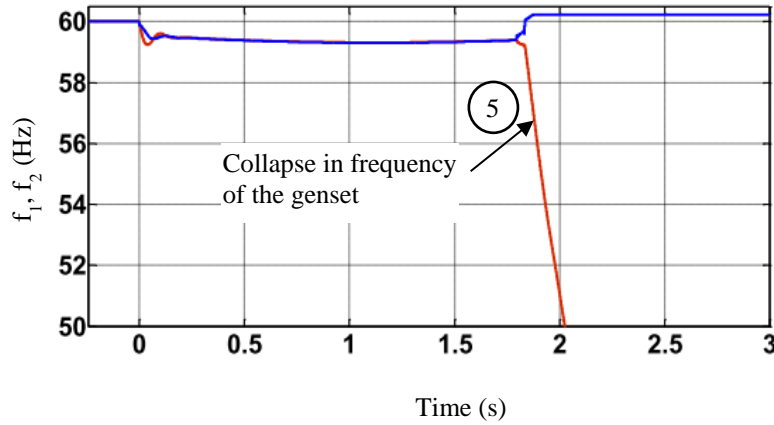


Figure 4.4 Simulation plot showing the frequency collapse in the genset (DER-1) of the mixed source microgrid for a 75–150 kW step load application.

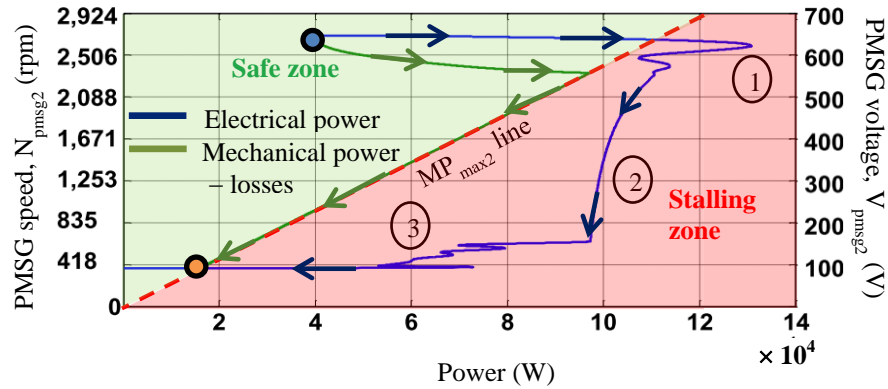


Figure 4.5 Locus of the PMSG speed and voltage vs. power characteristics for the inverter-based DER (DER-2) in the mixed source microgrid for a 75–150 kW step load application.

the transient load taken at the instant of load change by the inverter-based DER has caused prime-mover stalling ①, which led to its voltage collapse ② and the inverter dropped-off (i.e., tripped) ③. Then, the entire load burden of 150 kW fell on the genset, thereby overloading it ④ (cf. Figures 4.2–4.4). Since 150 kW load is more than the rated maximum capability of genset per the engine fuel map (cf. Figure 2.2 [31]), the genset has also experienced prime-mover stalling. This led to frequency collapse in the genset

⑤, and so it dropped-off in the end ⑥. Thus, the microgrid system has crashed upon the 75–150 kW load change application.

4.3 Prevention of DER Prime-mover Stalling in a Mixed Source Microgrid

In the earlier section, after unfolding the events following a 75–150 kW load change in the mixed source microgrid, it became clear that at first the inverter-based DER experienced prime-mover stalling that resulted in a cascading failure. The root cause of the problem is the slow response of genset isochronous governor. Due to its sluggish isochronous governor response, the genset could not restore the frequency soon enough to ease the load burden of inverter-based DER [28]. When the frequency dropped in response to the load change event, the inverter-based DER was hit with a peak load demand that caused prime-mover stalling that resulted in a voltage collapse.

4.3.1 Modified Power–frequency ($P-\omega$) droop controller for inverter-based DER

The DER prime-mover stalling in mixed source microgrid can be resolved in many ways. In the microgrid under study (cf. Figure 4.1), a solution would be to move the transient load burden from the inverter-based DER to the synchronous generator-based DER. With this goal in mind, a modified controller architecture using lead/lag controls is proposed for the inverter-based DER.

In the inverter-based DER, the traditional active power–frequency ($P-\omega$) droop controller has a constant droop gain, b_{p1} [2]. Table 4.1 shows the transfer function of the proposed controller, and equations governing frequency response to a step change in

Table 4.1 Difference between the frequency response of traditional and modified P - ω droop controller

P-ω droop controller	Frequency response to a step change of DER-2 power output is given by
<i>Traditional:</i> b_{p2}	$\Delta\omega_2(t) = -b_{p2}\Delta P_2(t)$
<i>Modified:</i> $b_{p2} \left(\frac{1 + sT_{n2}}{1 + sT_{d2}} \right)$	$\Delta\omega_2(t) = -b_{p2} \left(1 + \frac{T_{n2} - T_{d2}}{T_{d2}} e^{-t/T_{d2}} \right) \Delta P_2(t)$ $\Delta\omega_2(t = 0^+) = -b_{p2} \left(\frac{T_{n2}}{T_{d2}} \right) \Delta P_2$ $\Delta\omega_2(t \rightarrow \infty) = -b_{p2} \Delta P_2$

electrical load. A block diagram of the modified P-ω droop controller is illustrated in Figure 4.6 [28]. The frequency droop characteristics are displayed in Figure 4.7, where the transient droop curve is represented by the dashed line and the steady state droop curve by the solid line. An increase in the ratio (T_{n2}/T_{d2}) will further raise the slope of the transient droop curve, i.e., ($\Delta\omega_2/\Delta P_2 @ (t = 0^+)$), thereby decreasing the DER's transient load sharing. This enables the inverter-based DER to transfer a portion of its transient load burden to the genset.

The modified droop controls are tested for the same loading conditions in the mixed source microgrid of Figure 4.1, i.e., 75–150 kW, which resulted in a system shutdown earlier. The values of droop controller parameters for inverter-based DER, viz., T_{n2} and T_{d2} , used in simulation are given in Table 4.2. It should be noted that since the aim is

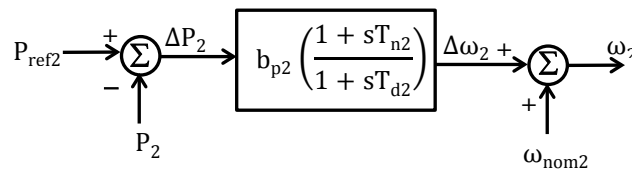


Figure 4.6 Block diagram of inverter-based DER's modified power-frequency (P-ω) droop controller using lead/lag controls

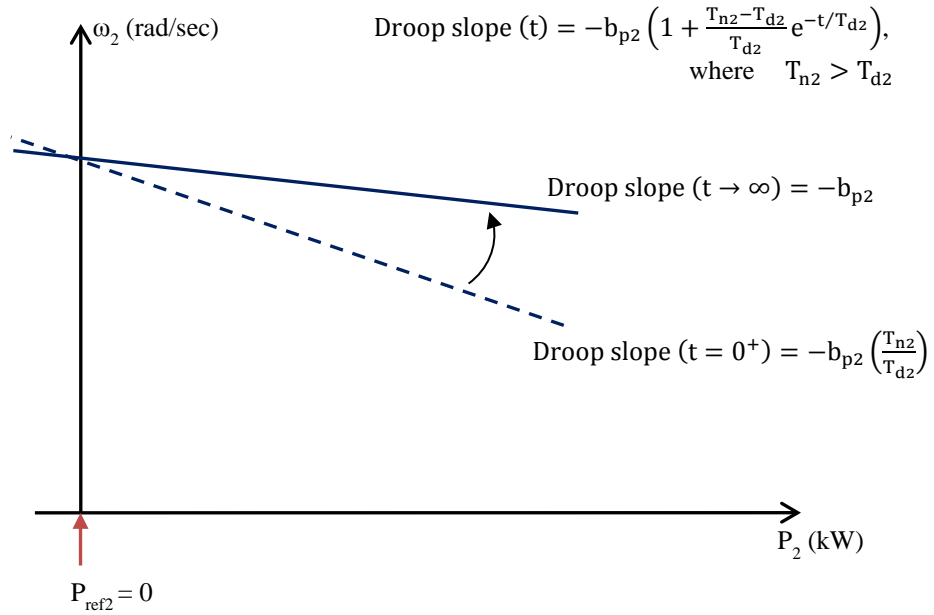


Figure 4.7 Transient and steady state frequency droop curves of the inverter-based DER with modified power-frequency (P- ω) controls.

Table 4.2 Lead/lag transfer function based modified droop controller settings

DER-k	T_{nk} (s/rad)	T_{dk} (s/rad)	b_{pk} (rad/s/ P_{pu})
DER-2	4	1	$2*\pi$
DER-1	Isochronous governor		

to change the transient load sharing and not the steady state, the value of b_{p2} parameter is the same as before. Figure 4.8 shows the simulation results for this test. Before the load change event, the original load of 75 kW is equally split between the two DERs. When another 75 kW load is added to the system, the peak (transient) load shared by inverter-based DER was limited to about 100 kW, which did not cause stalling of its prime-mover. This is further illustrated by the prime-mover speed and PMSG voltage vs. power characteristics shown in Figure 4.9.

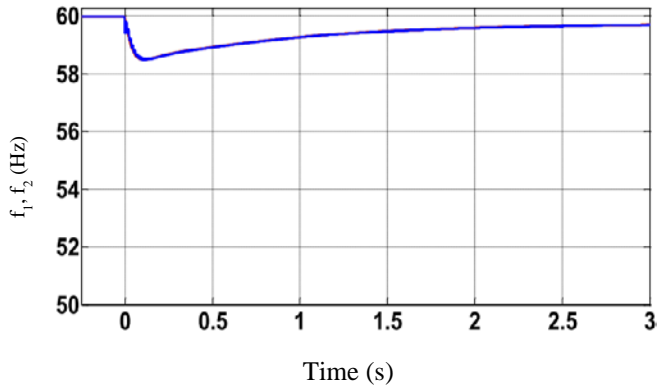
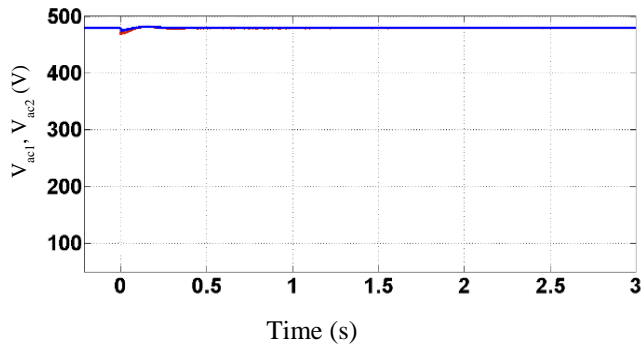
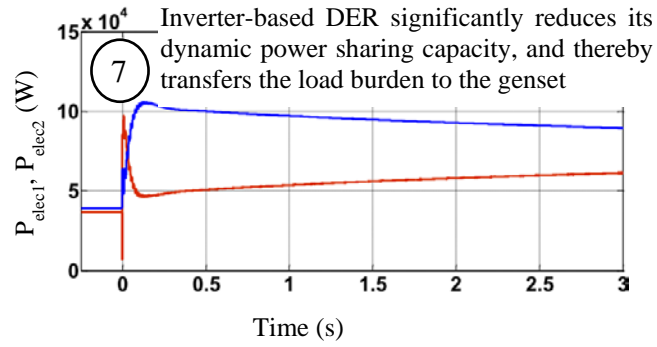


Figure 4.8 Simulation plots illustrating the system dynamic response for a 75–150 kW step change in electrical load. DER-1 (genset in red): isochronous governor; DER-2 (inverter-based DER in blue): $P_{ref2} = 37.5$ kW, $P_{max2} = 100$ kW.

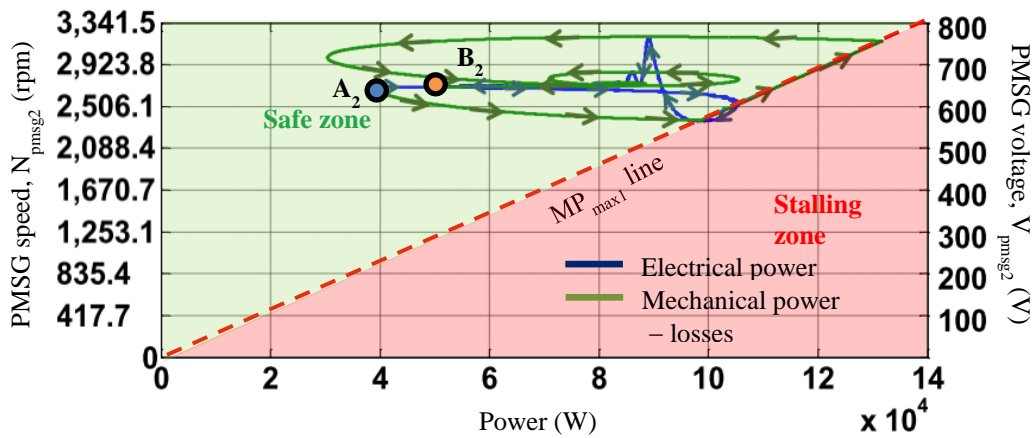


Figure 4.9 Locus of the PMSG speed and voltage vs. power characteristics for the inverter-based DER in the mixed source microgrid for a 75–150 kW step load application

As seen in Figures 4.8 and 4.9, the modified droop controller of inverter-based DER ensures that the electrical power trajectory stays within the *Safe zone*. Figures 4.10 (a) and (b) highlight the distinct frequency response characteristics of inverter-based DER and genset during this test. It is clear from the results that the proposed controls can be a viable option in preventing the prime-mover stalling in the inverter-based DER.

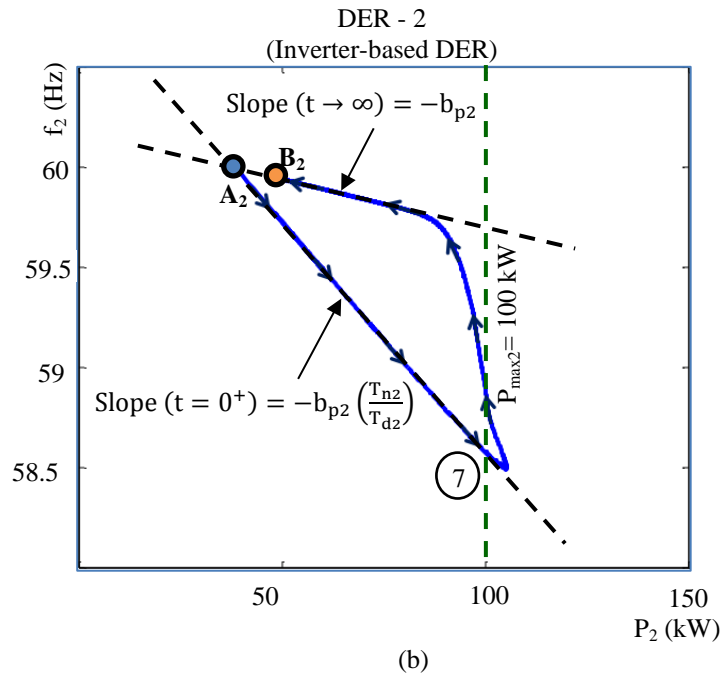
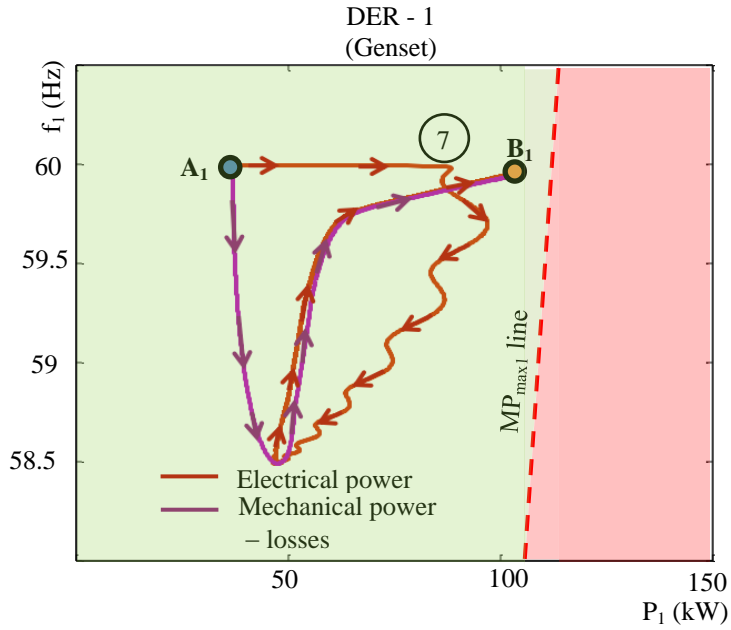


Figure 4.10 Results showing the performance of the proposed controller for 75–150 kW load change. DER₁ (synchronous generator in red): isochronous governor; DER₂ (inverter in blue): $P_{ref2} = 37.5$ kW, $P_{max2} = 100$ kW. See Figure 4.8 for the description of event ⑦.

4.4 Prevention of DER Prime-mover Stalling Through Governor Controls

In the last section, the prime-mover stalling in an inverter-based DER was prevented by changing its power-frequency ($P-\omega$) droop controller. This worked in a mixed source microgrid scenario since the transient load burden is transferred to another DER; but it would be ineffective in the standalone mode of operation. Hence, other alternatives such as the governor controls are explored for resolving the prime-mover stalling problem in standalone systems [23].

Consider the standalone operation of the genset that was tested earlier in Section 2.2. The prime-mover stalling took place for a 0–90 kW step load application to the genset (cf. Figure 2.4). An investigation of the speed governor closed loop control system (cf. Figure 1.2) reveals that the generator speed is influenced by various parameters related to governor and reciprocating engine model in addition to the synchronous generator parameters [23]. A few of these parameters like the machine inertia and friction coefficient (i.e., J_1 and B_1) and the engine delay are physically constrained. However, the electronic governor control gains could be programmed easily. Indeed the governor gains were optimized to improve the engine performance earlier in [35]. Hence, the governor control gains can be adjusted to prevent prime-mover stalling too [23].

In this study, once again the 0–90 kW step load change is applied to the genset. Two values of governor PID controller’s proportional gain (K_{pg1}) are tested, viz., 15 and 24. Figure 4.11 shows the locus of genset speed vs. power characteristics. The original value of $K_{pg1} = 15$ was established from the model validated in the CERTS Microgrid experimental tests (cf. Figure 1.3). However, by trial and error approach in the simulation model, $K_{pg1} = 24$ gave desirable response for a 0–90 kW step load change. In essence,

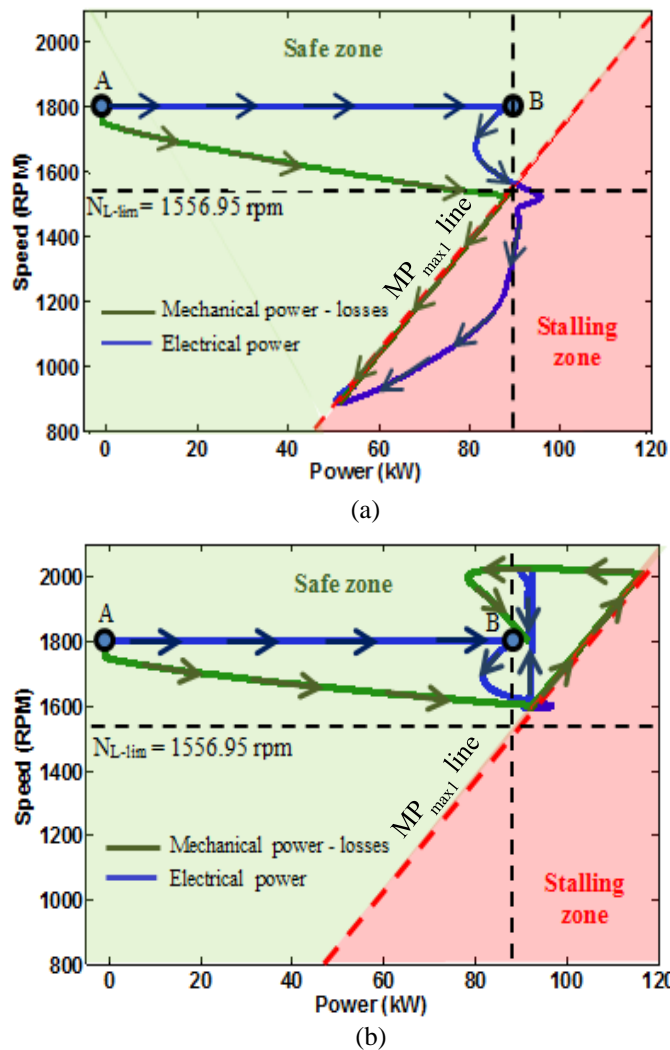


Figure 4.11 Locus of the genset speed vs. power characteristics for a 0–90 kW step load application. Governor PID controller’s proportional gain is set at (a) $K_{pg1} = 15$, and (b) $K_{pg1} = 24$

the higher governor loop gain increased the bandwidth to produce a quicker speed response in the genset. It helps counter the torque production delays in the natural gas engine. The same approach can be employed in the isochronous governor of inverter-based DER to prevent stalling of its prime-mover.

However, it should be noted that the high loop gain in engine governor controls might not be practical or it may have adverse effects on the engine emissions. Further experimental testing and feasibility studies are recommended in establishing the optimal controller gains for the governor.

4.5 Summary

When multiple DERs are integrated in a microgrid, these DERs are expected to share with each other their surplus marginal capacity so that no one will get overloaded. However, this did not happen in a particular test carried out at the CERTS Microgrid, i.e., a mixed source microgrid comprising genset and inverter-based DER. It was found that the slow acting governor controls of genset did not rescue the inverter-based DER from its prime-mover stalling. A large load change caused voltage collapse in the inverter-based DER and led to a cascading failure of the microgrid. The stalling problem can be prevented in a mixed source microgrid by a coordinated control strategy, which uses modified droop controls for the inverter-based DER. Alternatively, design changes are suggested to the engine governor controls of DER units.

CHAPTER 5

CONCLUSION AND FUTURE WORK

5.1 Conclusion

A microgrid provides the framework for integration and coordination of distributed energy resources (DERs). It can operate either in the grid-connected or islanded mode. However, the islanded mode of operation presents several challenges to the microgrid survivability. In particular, adverse conditions are observed in an islanded microgrid when large and fluctuating loads are supplied from numerous smaller-rated DERs. Similar conditions happen during loss of generation from a few DERs in the microgrid causing an abrupt change in net load for the surviving DERs. If these DERs cannot sustain the net load change, they lead the entire microgrid system to a cascading failure.

This report starts with the development of dynamic models for two kinds of prime-mover driven DERs, viz., synchronous generator-based DER (also known as ‘genset’) and inverter-based DER. Such models could be used in analyzing various system scenarios of higher DER penetration, which maybe otherwise impractical to do actual testing due to resource limitations in the field test bed.

For large and fluctuating loads close to the DER kW-rating, both the synchronous generator-based and inverter-based DERs are found to be susceptible to stalling behavior of their prime-movers. The root cause of stalling behavior is the slow response of engine governor that restores the prime-mover speed following a load change. Due to the lower

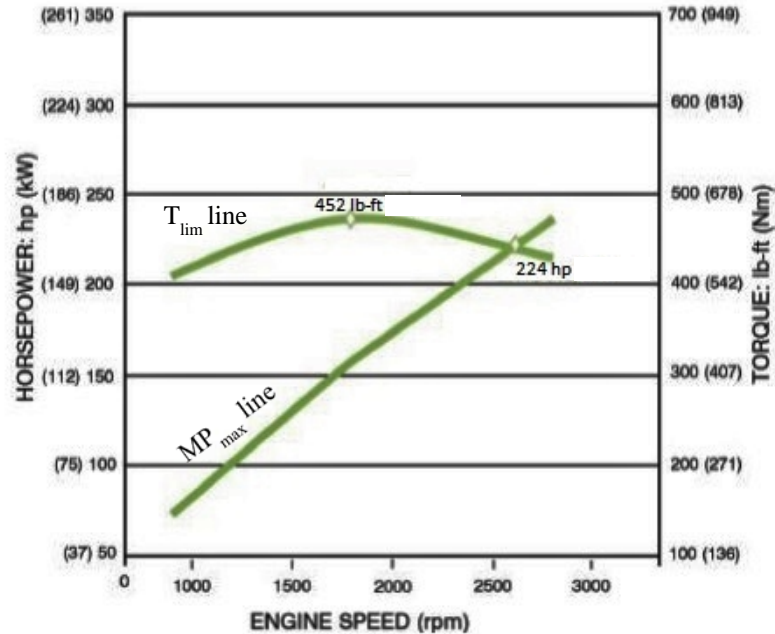


Figure 2.2 Fuel map of GM 8.1L natural gas engine typically used in a genset [31]

inertia of DERs employed in a microgrid system, their prime-mover speed undergoes huge swings upon a large disturbances. At lower speeds, the engine power is derated as illustrated by the engine fuel map shown in Figure 2.2. Thus, the mechanical power production of engine is limited by the MP_{max} line. The engine fuel map limit (MP_{max} line) is the hardware limit for mechanical power production from engine. Any electrical load demand exceeding the MP_{max} value would result in prime-mover stalling.

It is found that the prime-mover stalling in genset causes a frequency collapse in the microgrid. By contrast, the same condition in inverter-based DER results in a voltage collapse. This is because the inverter-based DER has an additional power conditioning stage after the synchronous generator.

When multiple DERs are integrated in a microgrid, these DERs are expected to share with each other their surplus marginal capacity so that no one will get overloaded. Two

microgrid case studies in Chapter 3 demonstrated this fact. However, it did not work out in a particular test carried out at the CERTS Microgrid, i.e., a mixed source microgrid comprising genset and inverter-based DER (cf. Chapter 4). It was found that the slow acting governor controls of genset did not rescue the inverter-based DER from its prime-mover stalling. This caused a voltage collapse in the inverter-based DER and led to a cascading failure of the microgrid. Graphical and analytical methods are proposed in this report to analyze the microgrid operation and performance under the boundary conditions.

To prevent the prime-mover stalling in DERs, design changes are suggested to engine governor controls. Alternatively, for an inverter-based DER operating in a mixed source microgrid, a modified active power-frequency ($P-\omega$) droop controller can be a viable option. The ultimate goal is to improve the coordination between DERs in the microgrid.

5.2 Suggested Future Work

5.2.1 *Feasible solutions for prevention of prime-mover stalling in DERs*

One of the critical problems encountered in an islanded microgrid is the DER prime-mover stalling — even a single DER in the microgrid experiencing this problem can cause the collapse of the entire microgrid system. To avoid this problem in a microgrid, the CERTS P_{\max} controls can be applied. It may need adjustments to the existing approach to achieve a feasible solution. Otherwise, two alternative strategies were presented in Chapter 4 with promising simulation results. However, experimental tests

are essential to find practical and widely deployable solutions that are easy to implement in commercial off-the-shelf DER equipment.

5.2.2 Role of smart loads and energy storage in microgrid applications

Smart loads are the variable loads that can be shed and restored in a flexible manner. Initial studies showed that the smart loads and energy storage could provide frequency regulation in the microgrid. Therefore, they can be effective in solving the prime-mover stalling of DERs in microgrid. Further studies are necessary to find economically viable solutions to install smart loads or energy storage in the microgrid.

5.2.3 Large scale microgrid simulation studies

The simulation studies carried out so far studied system integration problems in microgrids comprising two or three DERs, smart loads and energy storage. However, the ultimate aim is to develop modular and scalable microgrid solutions deployable in various communities. Hence, it is imperative to conduct simulation studies on a benchmark distribution system such as 33-bus or 69-bus system. This would help in easy evaluation and integration of developed solutions by the broader research community.

Appendix A

Simulation model parameters for the synchronous generator-based DER (i.e., genset)

Table A.1 CERTS control parameters

Parameter	Symbol	Value	Units
P- ω droop gain	b_{p1}	1.885	rad/s/P_{pu}
Q-V droop gain	b_{q1}	0.15	V_{pu}/Q_{pu}
P_{max} controller proportional gain	K_{p_Pmax1}	0	rad/s/P_{pu}
P_{max} controller integral gain	K_{i_Pmax1}	30	$\text{rad/s}^2/P_{pu}$
Power maximum	P_{max1}	1	pu

Table A.2 Governor, engine and shaft model parameters

Parameter	Symbol	Value	Units
Governor proportional gain	K_{pg1}	15	T_{pu}/ω_{pu}
Governor integral gain	K_{ig1}	20	$T_{pu}/\omega_{pu}/s$
Engine torque delay	t_{d1}	0.0416	s
Engine torque limit	T_{lim1}	552	N.m
Moment of inertia	J_1	2.86	kg.m^2
Frictional coefficient	B_1	0.001	$\text{kg.m}^2/s$

Table A.3 AC8B exciter model parameters

Parameter	Symbol	Value	Units
Exciter time constant	τ_{e1}	0.1	s
Exciter constant related to self-excited field	K_{e1}	1	NA
Exciter saturation function	S_{e1}	0	NA
DVR proportional gain	K_{pe1}	60	V_{pu}/V_{pu}
DVR integral gain	K_{ie1}	40	$V_{pu}/V_{pu}/s$
DVR derivative gain	K_{de1}	0.2	$V_{pu}.s/V_{pu}$

Table A.4 Synchronous generator model parameters

Parameter	Symbol	Value	Units
Rated apparent power	S_{rat1}	225	kVA
Rated voltage	V_{ll1}	480	V
Synchronous speed	N_s	1800	rpm
Synchronous reactance	X_d	2.877	pu
Transient reactance	X_d'	0.184	pu

Appendix B

Simulation model parameters for the inverter-based DER

Table B.1 Parameters of CERTS controls

Parameter	Symbol	Value	Units
P- ω droop gain	b_{p2}	3.77	rad/s/P _{pu}
Q-V droop gain	b_{q2}	0.15	V _{pu} /Q _{pu}
P _{max} controller proportional gain	K_{p_Pmax2}	0	rad/s/P _{pu}
P _{max} controller integral gain	K_{i_Pmax2}	30	rad/s ² /P _{pu}
Power maximum	P _{max2}	1	pu

Table B.2 Governor, engine and shaft model parameters

Parameter	Symbol	Value	Units
Governor proportional gain	K_{pg2}	3.7	T _{pu} / ω_{pu}
Governor integral gain	K_{ig2}	5	T _{pu} / ω_{pu} /s
Engine torque delay	t_{d2}	0.0416	s
Engine torque limit	T _{lim2}	398	N.m
Moment of inertia	J ₂	1	kg.m ²
Frictional coefficient	B ₂	0.001	kg.m ² /s

Table B.3 Permanent magnet synchronous generator model parameters

Parameter	Symbol	Value	Units
Rated apparent power	S_{rated2}	125	kVA
Rated voltage	V_{ll2}	600	V
Rated RPM	N_r	3000	rpm
EMF constant	K_e	1.32	V/rad/s

Table B.4 Filter and transmission line parameters

Parameter	Symbol	Value	Units
Filter reactance	X_L	3	%
Transformer reactance	X_T	5	%
Cable reactance	X_{cab1}	0.1	%
Cable reactance	X_{cab2}	2	%

References

- [1] R. H. Lasseter, J. H. Eto, B. Schenkman, J. Stevens, H. Vollkommer, D. Klapp, E. Linton, H. Hurtado, and J. Roy, “CERTS Microgrid Laboratory Test Bed,” *IEEE Trans. Power Deliv.*, vol. 26, no. 1, pp. 325–332, Jan. 2011.
- [2] R. H. Lasseter and P. Piagi, “Microgrid: a conceptual solution,” in *2004 IEEE 35th Annual Power Electronics Specialists Conference*, 2004, vol. 6, pp. 4285–4290.
- [3] H. Nikkhajoei and R. H. Lasseter, “Distributed generation interface to the CERTS microgrid,” *IEEE Trans. Power Deliv.*, vol. 24, no. 3, pp. 1598–1608, 2009.
- [4] “Inverter-Based Cogeneration InVerdē, INV-100.” [Online]. Available: <http://www.tecogen.com/products-cogeneration-inv-100.htm>. [Accessed: 12-Apr-2016].
- [5] “InVerdē INV-100 CHP Module,” *Operation & Maintenance Manual*. TECOGEN Inc., Waltham, MA, 2009.
- [6] D. Klapp, R. Zimmerly, and J. Howard, “CERTS Microgrid, Tecogen InVerdē INV 100 Test Report,” 2012. [Online]. Available: <http://energy.lbl.gov/ea/certs/pdf/aep-tecogen-inverde-100.pdf>. [Accessed: 11-Apr-2016].
- [7] S. Krishnamurthy, T. M. Jahns, and R. H. Lasseter, “The operation of diesel gensets in a CERTS microgrid,” in *2008 IEEE Power and Energy Society General Meeting*, 2008.
- [8] A. Gangopadhyay and P. Meckl, “Modeling, validation and system identification

- of a natural gas engine,” in *Proceedings of the 1997 American Control Conference*, 1997, vol. 1, pp. 294–298.
- [9] “IEEE Recommended Practice for Excitation System Models for Power System Stability Studies,” *IEEE Std 421.5-2005*. pp. 1–85, 2006.
- [10] “DECS 250,” *Instruction Manual for Digital Excitation Control System*. Basler Electric, Highland, IL.
- [11] “Synchronous Generator - Typical Dynamic Characteristics,” *431CSL6204 Generator*. [Online]. Available: <http://www.marathonelectric.com/generators/docs/perf/431CSL6204T60.pdf>. [Accessed: 12-Apr-2016].
- [12] A. A. Renjit, M. S. Illindala, and D. A. Klapp, “Graphical and Analytical Methods for Stalling Analysis of Engine Generator Sets,” *IEEE Trans. Ind. Appl.*, vol. 50, no. 5, pp. 2967–2975, Sep. 2014.
- [13] A. A. Renjit, M. S. Illindala, R. H. Lasseter, M. J. Erickson, and D. Klapp, “Modeling and control of a natural gas generator set in the CERTS microgrid,” in *Energy Conversion Congress and Exposition (ECCE), 2013 IEEE*, 2013, pp. 1640–1646.
- [14] A. A. Renjit, M. S. Illindala, and D. A. Klapp, “Modeling and analysis of the CERTS microgrid with natural gas powered distributed energy resources,” in *Industrial & Commercial Power Systems Technical Conference (I&CPS), 2015 IEEE/IAS 51st*, 2015, pp. 1–8.
- [15] M. J. Ryan and R. D. Lorenz, “A ‘power-mapping’ variable-speed control

- technique for a constant-frequency conversion system powered by a IC engine and PM generator,” in *2000 IEEE Industry Applications Society Annual Meeting*, 2000, vol. 4, pp. 2376–2382.
- [16] M. Kimura, H. Koharagi, K. Imaie, S. Dodo, H. Arita, and K. Tsubouchi, “A permanent magnet synchronous generator with variable speed input for co-generation system,” in *2001 IEEE Power Engineering Society Winter Meeting. Conference Proceedings*, 2001, vol. 3, pp. 1419–1424.
- [17] Hyunjae Yoo, Byung-Geuk Cho, Seung-Ki Sul, Sang-Min Kim, and Yongho Park, “A power flow control strategy for optimal fuel efficiency of a variable speed engine-generator based series hybrid electric vehicle,” in *2009 IEEE Energy Conversion Congress and Exposition*, 2009, pp. 443–450.
- [18] A. R. Cooper, D. J. Morrow, and K. D. R. Chambers, “Development of a diesel generating set model for large voltage and frequency transients,” in *IEEE PES General Meeting*, 2010, pp. 1–7.
- [19] G. Quionez-Varela and A. Cruden, “Development of a Small-Scale Generator Set Model for Local Network Voltage and Frequency Stability Analysis,” *IEEE Trans. Energy Convers.*, vol. 22, no. 2, pp. 368–375, Jun. 2007.
- [20] K. D. R. Chambers, D. J. McGowan, and D. J. Morrow, “A Digital Load Relief Scheme for a Diesel Generating Set,” in *2007 IEEE Power Engineering Society General Meeting*, 2007, pp. 1–7.
- [21] C. L. Haller, D. L. Harris, and R. T. Fink, “Modeling of Emergency Diesel Generator and Governor Transient Response Using MATLAB/SIMULINK,” SAE

Technical Paper, 1995.

- [22] A. Mondal, D. A. Klapp, M. S. Illindala, and J. H. Eto, “Modeling, analysis and evaluation of smart load functionality in the CERTS Microgrid,” in *Energy Conversion Congress and Exposition (ECCE), 2014 IEEE*, 2014, pp. 4628–4634.
- [23] A. Mondal, M. S. Illindala, A. A. Renjit, and A. S. Khalsa, “Analysis of limiting bounds for stalling of natural gas genset in the CERTS microgrid test bed,” in *Power Electronics, Drives and Energy Systems (PEDES), 2014 IEEE International Conference on*, 2014, pp. 1–5.
- [24] L. M. Tolbert, W. A. Peterson, M. B. Scudiere, C. P. White, T. J. Theiss, J. B. Andriulli, C. W. Ayers, G. Farquharson, G. W. Ott, and L. E. Seiber, “Electronic power conversion system for an advanced mobile generator set,” in *Industry Applications Conference, 2001. Thirty-Sixth IAS Annual Meeting. Conference Record of the 2001 IEEE*, 2001, vol. 3, pp. 1763–1768.
- [25] S.-H. Lee, J.-S. Yim, J.-H. Lee, and S.-K. Sul, “Design of speed control loop of a variable speed diesel engine generator by electric governor,” in *Industry Applications Society Annual Meeting, 2008. IAS’08. IEEE*, 2008, pp. 1–5.
- [26] J. Leuchter, V. Řeřucha, Z. Krupka, and P. Bauer, “Dynamic behavior of mobile generator set with variable speed and diesel engine,” in *Power Electronics Specialists Conference, 2007. PESC 2007. IEEE*, 2007, pp. 2287–2293.
- [27] R. Panora, J. E. Gehret, M. M. Furse, and R. H. Lasseter, “Real-World Performance of a CERTS Microgrid in Manhattan,” *IEEE Trans. Sustain. Energy*, vol. 5, no. 4, pp. 1356–1360, Oct. 2014.

- [28] A. A. Renjit, "Modeling, Analysis and Control of Mixed Source Microgrid," Ph.D. Dissertation, Electrical and Computer Engineering, The Ohio State University, Columbus, OH, 2015.
- [29] P. C. Krause, O. Wasynczuk, and S. D. Sudhoff, *Analysis of Electric Machinery and Drive Systems*. Wiley-IEEE Press, 2002.
- [30] A. E. Fitzgerald, C. Kingsley, and S. D. Umans, *Electric Machinery*, 6th ed. McGraw-Hill, New York, NY, 2003.
- [31] "Datasheet of GM 8.1L Vortec Engine." [Online]. Available: [http://www.rotatingright.com/pdf/8.1 Litre Brochure.pdf](http://www.rotatingright.com/pdf/8.1%20Litre%20Brochure.pdf). [Accessed: 12-Apr-2016].
- [32] A. Mondal, M. Illindala, A. Khalsa, D. Klapp, and J. Eto, "Design and Operation of Smart Loads to Prevent Stalling in a Microgrid," *IEEE Trans. Ind. Appl.*, vol. 52, no. 2, pp. 1–1, 2016.
- [33] A. J. Wood and B. F. Wollenberg, *Power generation, operation, and control*. John Wiley & Sons, New York, NY, 2012.
- [34] A. D. Paquette, M. J. Reno, R. G. Harley, and D. M. Divan, "Sharing Transient Loads: Causes of Unequal Transient Load Sharing in Islanded Microgrid Operation," *IEEE Ind. Appl. Mag.*, vol. 20, no. 2, pp. 23–34, Mar. 2014.
- [35] D. J. McGowan, D. J. Morrow, and M. McArdle, "A digital PID speed controller for a diesel generating set," in *2003 IEEE Power Engineering Society General Meeting*, 2003, vol. 3, pp. 1472–1477.